and GAPDH) or 1.2% (Ago2) agarose gels and visualized under UV illumination after staining with ethidium bromide.

Western blotting. Anti-human Ago2 rabbit polyclonal antibody (Upstate, Lake Placid, NY), anti-actin rabbit polyclonal antibody (Sigma–Aldrich), anti-GAPDH mouse monoclonal antibody (GeneTex Inc., San Antonio, TX), peroxidase-conjugated anti-rabbit IgG polyclonal antibody (Santa Cruz Biotechnology, Santa Cruz, CA), and peroxidase-conjugated anti-mouse IgG polyclonal antibody (Santa Cruz Biotechnology) were purchased. The nucleotide sequences of siRNA for GAPDH (siGAPDH) with a 2-nucleotide overhang (underline) were 5′-CCAAAUAUGAUGACAUCAAGAAGGUAG-3′ (sense) and 5′-ACCUUCUUGAUGUCAUCAUAUUUGGAU-3′ (antisense). The sequences of siGAPDH correspond to the nucleotide region 791–815.

Cell extracts were prepared with lysis buffer composed of 10 mM Tris (pH 7.5), 0.1% SDS, 50 μg/ml aprotinin, 200 μM leupeptin, 2 mM PMSF, and 100 μM pepstatin A. Total protein concentration was measured by using a BCA Protein Assay Reagent Kit. The cell extract was subjected to 10 or 15% SDS–PAGE and transferred electrophoretically to a polyvi-

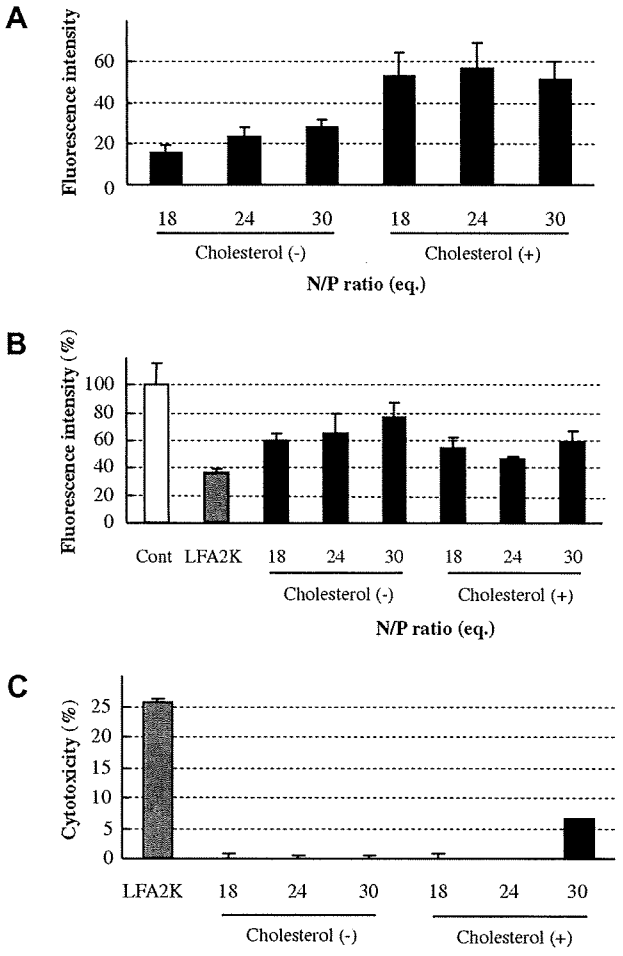

Fig. 1. Preparation of siRNA/PCLs complexes for siRNA transfection. (A) The amount of siRNA taken into HT1080 cells was determined after FAM-labeled siRNA/PCLs complexes had been allowed to interact with these cells for 4 h at 37 °C. PCLs with or without cholesterol were prepared and mixed with FAM-labeled siRNA at the various *N/P* ratios indicated in the figure. The fluorescence intensities of FAM in the cells were corrected for protein content. (B) RNAi efficiencies obtained by using PCLs were determined by conducting a quantitative gene silencing experiment. EGFP/HT-1080 cells were transfected with siEGFP complexed with PCLs (closed bar) or LFA2K (gray bar). The fluorescence intensity of EGFP was determined at 48 h post-transfection and corrected for protein content. The fluorescence intensity indicated as control (Cont, open bar) was that of cells not transfected with siRNA. Data represent the percent of control fluorescence intensity. (C) Cytotoxicity of PCLs against EGFP/HT1080 cells was determined. PCLs (closed bar) or LFA2K (gray bar) carrying siEGFP were allowed to interact with EGFP/HT1080 cells for 4 h at 37 °C and then removed. After further 24-h incubation, cell viability was estimated by conducting a modified MTT assay using Tetracolor ONE™. The percentage of damaged cells was calculated by setting non-treated cells as the control.

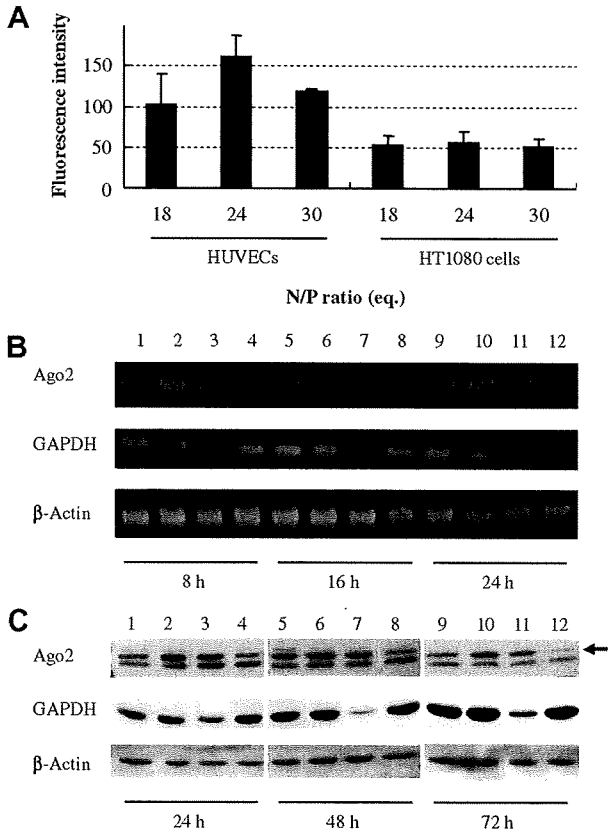

Fig. 2. Ago2 knockdown in HUVECs. (A) The amount of siRNA taken into HUVECs or HT1080 cells was determined after FAM-labeled siRNA/PCL complexes were allowed to interact with these cells for 4 h at 37 °C. PCLs composed of cetyl-PEI, DOPE, and cholesterol were prepared and mixed with FAM-labeled siRNA at the various *N/P* ratios indicated in the figure. The fluorescence intensities of FAM in the cells were corrected for protein content. (B) RT-PCR was performed by using HUVECs transfected with siAgo2 or siGAPDH. Total RNAs were isolated at 8, 16, and 24 h post-transfection, reverse transcribed, and applied to PCR using an Ago2, GAPDH or β-actin primer set. The PCR products were visualized by ethidium bromide under UV illumination. Lanes 1, 5, and 9, control without siRNA; lanes 2, 6, and 10, SiEGFP used as a non-silencing control; lanes 3, 7, and 11, SiGAPDH used as a control siRNA; and lanes 4, 8, and 12, SiAgo2. (C) Western blotting was performed by using HUVECs transfected with siAgo2 or siGAPDH. Cell extracts were prepared at 24, 48 or 72 h post-transfection. Ten micrograms of total protein was separated and incubated with anti-Ago2 rabbit polyclonal antibody, anti-actin rabbit polyclonal antibody or anti-GAPDH mouse monoclonal antibody. SiEGFP was used as non-silencing control; and siGAPDH, as control siRNA. Arrow shows the location of Ago2 protein. Lanes 1, 5, and 9, control without siRNA; lanes 2, 6, and 10, SiEGFP used as a non-silencing control; lanes 3, 7, and 11, SiGAPDH used as a control siRNA; and lanes 4, 8, and 12, SiAgo2.

nylidene difluoride (PVDF) membrane (MILLIPORE, Billerica, MA). After having been blocked for 1 h at room temperature with 5% skim milk in Tris–HCl-buffered saline containing 0.1% Tween 20 (TTBS, pH 7.4), the membrane was incubated with a primary antibody (β-actin and GAPDH; 0.1 μg/ml, Ago2; 2 μg/ml) for 2 h at room temperature. Then, it was incubated with a peroxidase-conjugated secondary antibody at a dilution of 1:10,000 for 1 h at room temperature. Each sample was developed by using a chemiluminescent substrate (ECL; Amersham Biosciences).

Cell growth assay. HUVECs were seeded onto 24-well plates at the density of 5×10^4 cells/dish and transfected with siAgo2 or siEGFP complexed with PCLs. After 0-, 24- or 48-h incubation, Tetracolor ONE™ was added to each well in accordance with the manufacturer's instructions. The amount of formazan formed in 2 h was measured by the microplate reader at a test wavelength of 492 nm and a reference wavelength of 630 nm.

Detection of apoptotic cells. HUVECs were seeded onto 35-mm dishes at the density of 2.5×10^5 cells/dish and transfected with siAgo2/ or siEGFP/PCL complexes. At 48 h after transfection, TUNEL staining was performed by using an ApopTag Plus Fluorescein In Situ Apoptosis Detection Kit (Chemicon International, Temecula, CA) according to the manufacturer's instructions. These cells were counterstained with DAPI and observed under an LSM510 META confocal Laser-Scanning-Microscope (Carl Zeiss, Oberkochen, Germany).

Tube formation assay. Matrigel (BD Biosciences Bedford, MA) was diluted to 4 mg/ml with EGM-2, added to 24-well plates, and allowed to undergo polymerization. HUVECs (5×10^5 cells/well) transfected with siAgo2 or siEGFP complexed with PCLs were then added to each well and incubated for 6 h at 37 °C. Photomicrographs were taken in 10 fields/group with an Olympus IMT-2 microscope (Olympus, Tokyo, Japan). The length of tubes was calculated by using software Image J (NIH, Bethesda, MD).

Results

Preparation of siRNA/PCLs complexes for siRNA delivery

At first, the adequate formulation of PCLs for siRNA transfection was determined by evaluating the uptake amount of siRNA, the knockdown efficiency, and the cytotoxicity. The sizes of siRNA/PCLs complexes prepared in this study were in the range of 130–155 nm, and the ξ-potentials of them were 30–50 mV. The uptake experiment showed that the presence of cholesterol in PCLs enhanced the uptake amount of FAM-labeled siAgo2 into HT1080 cells (Fig. 1A). In addition, the highest siRNA uptake was achieved when the *N/P* ratio of siRNA/PCLs complex was 24 equivalents (equiv). In the quantitative knockdown experiment, the siRNA formulation most taken up by HT1080 cells also showed the maximal knockdown efficiency (Fig. 1B). The cytotoxicity of siRNA/PCLs complexes was much lower than that of LFA2K (Fig. 1C).

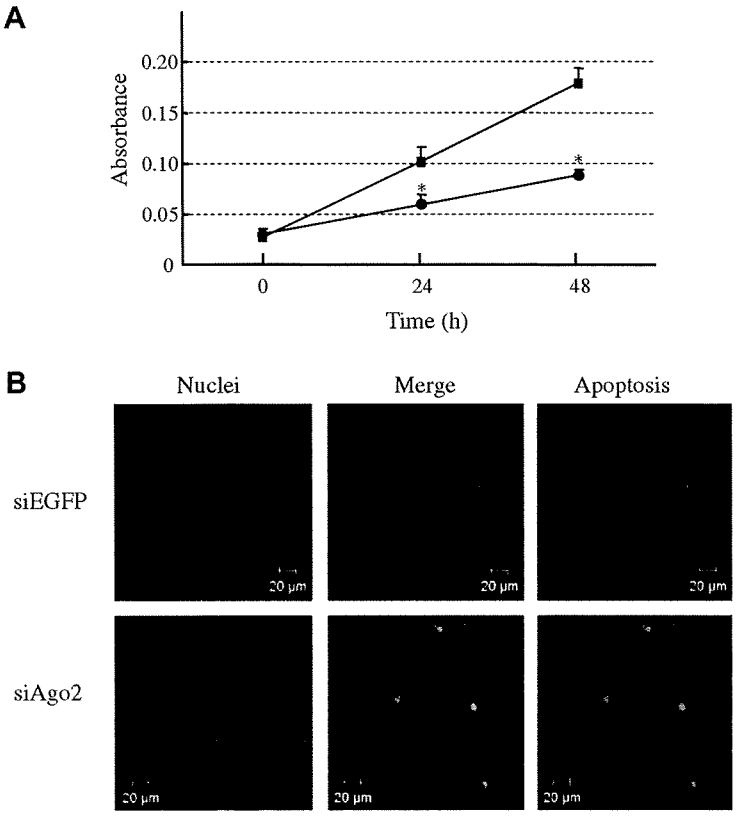

Fig. 3. Influence of Ago2 knockdown on the growth of HUVECs. (A) At 0, 24, and 48 h post-transfection, a modified MTT assay was performed with HUVECs transfected with siAgo2 (circles) or siEGFP (squares) complexed with PCLs. Data show the absorbance with SD bars. Significant differences from siEGFP group are indicated ($^*P < 0.01$). (B) Apoptosis of HUVECs transfected with siAgo2/PCL complexes was determined by TUNEL staining at 48 h post-transfection. The nuclei were counterstained with DAPI (blue). Apoptotic cells (FITC, green) were observed under an LSM510 META confocal Laser-Scanning-Microscope. Scale bars represent 20 μm.

Ago2 knockdown in HUVECs

To confirm Ago2 knockdown in HUVECs, these cells were transfected with siAgo2 (final concentration: 40 nM) complexed with PCLs. The uptake experiment indicated that the amount of FAM-labeled siAgo2 taken up was greater by HUVECs than by HT1080 cells (Fig. 2A). The optimal *N*/*P* ratio of siRNA/PCLs complexes for incorporating siRNA into HUVECs was 24 equiv, consistent with the result obtained for HT1080 cells. Based on these results from the formulation screening, we adopted the following formulation for use in subsequent experiments: cetyl-PEI/DOPE/cholesterol = 0.05/1/0.5 as a molar ratio, *N*/*P* ratio = 24 equiv. The RT-PCR data showed that siAgo2 down-regulated the expression of Ago2 mRNAs in HUVECs (Fig. 2B). The specificity of Ago2 knockdown was confirmed by the transfection with siEGFP or siGAPDH. Neither siEGFP nor siGAPDH affected the expression of Ago2 mRNA, and siGAPDH suppressed the expression of GAPDH mRNA. These data indicate that the knockdown of Ago2 occurred in a siAgo2-dependent manner. The Western blotting data demonstrated that the expression of Ago2 protein was actually diminished by siAgo2 transfection (Fig. 2C).

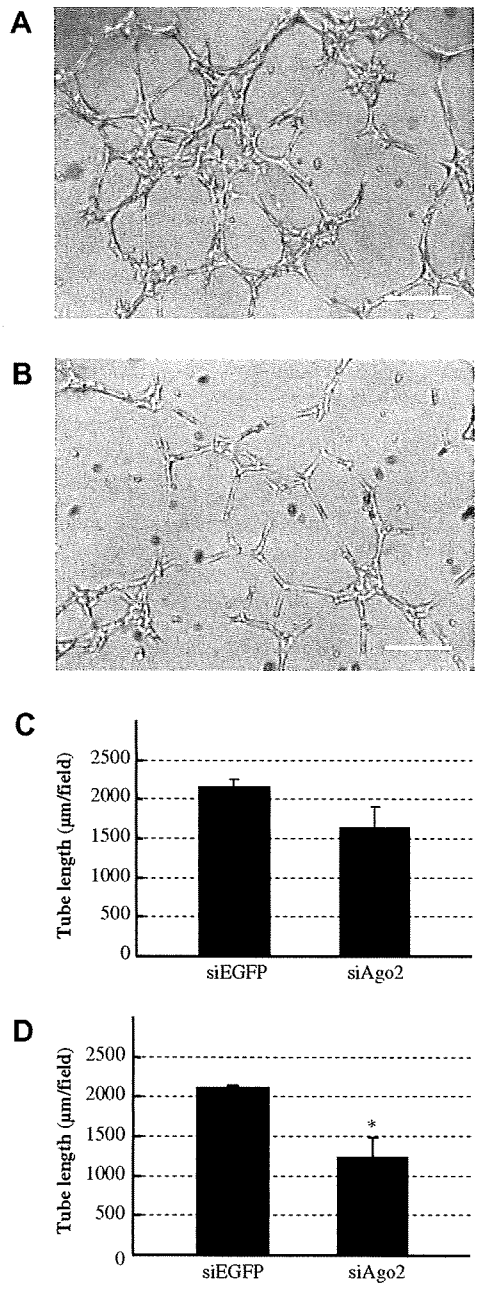

Fig. 4. Inhibition of tube formation by Argonaute2 knockdown. Tube formation assay was performed with HUVECs transfected with siAgo2/PCL complexes. The transfected cells were collected at 24 (C) or 48 h (A, B, and D) post-transfection and incubated on Matrigel for 6 h at 37 °C in 5% CO_2. (A, B) Photomicrographs show the tube formation of HUVECs transfected with siEGFP (A) or siAgo2 (B). Scale bars represent 20 μm. (C and D) The length of tubes was calculated by using the software Image J. Significant difference from siEGFP group is indicated ($^*P < 0.05$).

Influence of Ago2 knockdown on angiogenic potentials of HUVECs

To investigate the influence of Ago2 knockdown on the properties of endothelial cells, HUVECs were transfected with siAgo2/PCL complexes. The influence of Ago2 knockdown on the proliferation of HUVECs was determined by using a modified MTT assay. As shown in Fig. 3A, the treatment with siAgo2 significantly suppressed the growth of HUVECs in comparison to that with siEGFP, a control siRNA ($P < 0.001$). TUNEL staining showed that a certain population of HUVECs treated with siAgo2 underwent apoptosis at 48 h after the transfection (Fig. 3B). The percentage of apoptotic cells was about 20% in siAgo2-treated HUVECs. This result indicates that the growth inhibition by Ago2 knockdown was partially caused by the induction of apoptosis. On the other hand, Ago2 knockdown did not induce apoptosis of HT1080 cells in the similar experiment (Supplementary Fig. 1).

In the tube formation assay, the HUVECs transfected with siEGFP formed capillary-like structures (Fig. 4A). In contrast, the treatment with siAgo2 suppressed the tube formation of HUVECs (Fig. 4B). The length of tubes, an indicator of tube formation, was significantly reduced by the knockdown of Ago2 when HUVECs were used for this assay at 48 h post-transfection (Fig. 4C and D). These results indicate that siAgo2 inhibited indispensable events of angiogenesis.

Discussion

In the present study, we demonstrated that the knockdown of Ago2 resulted in the loss of the angiogenic potential of HUVECs, thus suggesting that Ago2 is required for angiogenesis. We consider one of the reasons to be indirect effects related to the miRNA system. The knockdown of Ago2 could affect the expression levels of some critical miRNAs required for the formation of angiogenic vessels.

For instance, it was reported that miR-221 and miR222 control the ability of HUVECs to form new capillaries [12]. However, the knockdown of Ago2 is considered to affect most miRNAs not just miR-221/2. As well as the knockdown of Ago2, the deletion of Dicer function resulted in failure of mouse embryonic angiogenesis [13]. These results indicate that the miRNA system is indispensable for angiogenesis, in which Ago2 also plays a critical role.

Angiogenesis is a crucial event for many severe diseases such as cancer. Therefore, the development of antiangiogenic RNAi therapy have been widely investigated [3]. The knockdown of angiogenic factor such as vascular endothelial growth factor is expected to be a novel therapeutic strategy [3]. Our data suggest that Ago2 might be a unique therapeutic target for antiangiogenic RNAi therapy. Since siAgo2 not only cleaves the mRNA of Ago2 but also occupies the protein of Ago2 that is required for RNAi, the use of siAgo2 is considered to be an efficient strategy to disturb an ordered miRNA system. The amount of Ago2 protein would not be rate determining in this strategy, whereas other siRNA requires sufficient Ago2 protein. Therefore, the knockdown of Ago2 is a unique approach for inhibiting angiogenesis. However, a siRNA delivery system that targets endothelial cells specifically is necessary to apply siAgo2 for antiangiogenic therapy, since siAgo2 would be expected to affect the entire miRNA system.

In the present study, we determined the optimal formulation of PCLs by determining the gene silencing efficiency and cytotoxicity and demonstrated PCLs to be a novel siRNA vector. PCLs carrying siAgo2 attenuated the angiogenic potential of HUVECs. In the case that PCLs carrying siAgo2 are applied *in vivo,* the availability of them will be extended by surface modification of the liposomes with functional molecules such as polyethyleneglycol and certain ligands targeting angiogenic endothelial cells. In our previous study, we demonstrated that Ala-Pro-Arg-Pro-Gly (APRPG) is a useful peptide for the active targeting of angiogenic vessels [17]. APRPG-modified liposomal doxorubicin actually caused effective tumor growth suppression through damaging angiogenic endothelial cells [17]. APRPG-modified liposomal siAgo2 might thus be a good candidate for use in antiangiogenic RNAi therapy.

Acknowledgments

This research was supported by Research on Advanced Medical Technology on Health and Labour Sciences Research Grants, Ministry of Health, Labour and Welfare, Japan.

Appendix A. Supplementary data

Supplementary data associated with this article can be found, in the online version, at doi:10.1016/j.bbrc.2008.01.074.

References

[1] A. Fire, S. Xu, M.K. Montgomery, S.A. Kostas, S.E. Driver, C.C. Mello, Potent and specific genetic interference by double-stranded RNA in *Caenorhabditis elegans*, Nature 391 (1998) 806–811.
[2] S.M. Elbashir, J. Harborth, W. Lendeckel, A. Yalcin, K. Weber, T. Tuschl, Duplexes of 21-nucleotide RNAs mediate RNA interference in cultured mammalian cells, Nature 411 (2001) 494–498.
[3] S.I. Pai, Y.Y. Lin, B. Macaes, A. Meneshian, C.F. Hung, T.C. Wu, Prospects of RNA interference therapy for cancer, Gene Ther. 13 (2006) 464–477.
[4] R.I. Gregory, T.P. Chendrimada, N. Cooch, R. Shiekhattar, Human RISC couples microRNA biogenesis and posttranscriptional gene silencing, Cell 123 (2005) 631–640.
[5] K. Okamura, A. Ishizuka, H. Siomi, M.C. Siomi, Distinct roles for Argonaute proteins in small RNA-directed RNA cleavage pathways, Genes Dev. 18 (2004) 1655–1666.
[6] J. Liu, M.A. Carmell, F.V. Rivas, C.G. Marsden, J.M. Thomson, J.J. Song, S.M. Hammond, L. Joshua-Tor, G.J. Hannon, Argonaute2 is the catalytic engine of mammalian RNAi, Science 305 (2004) 1437–1441.
[7] G. Meister, M. Landthaler, A. Patkaniowska, Y. Dorsett, G. Teng, T. Tuschl, Human Argonaute2 mediates RNA cleavage targeted by miRNAs and siRNAs, Mol. Cell 15 (2004) 185–197.
[8] C. Matranga, Y. Tomari, C. Shin, D.P. Bartel, P.D. Zamore, Passenger-strand cleavage facilitates assembly of siRNA into Ago2-containing RNAi enzyme complexes, Cell 123 (2005) 607–620.
[9] M. Cristofanilli, C. Charnsangavej, G.N. Hortobagyi, Angiogenesis modulation in cancer research: novel clinical approaches, Nat. Rev. Drug Discov. 1 (2002) 415–426.
[10] K. Shimizu, T. Asai, N. Oku, Antineovascular therapy, a novel antiangiogenic approach, Expert Opin. Ther. Targets 9 (2005) 63–76.
[11] N. Ferrara, K.J. Hillan, W. Novotny, Bevacizumab (Avastin), a humanized anti-VEGF monoclonal antibody for cancer therapy, Biochem. Biophys. Res. Commun. 333 (2005) 328–335.
[12] L. Poliseno, A. Tuccoli, L. Mariani, M. Evangelista, L. Citti, K. Woods, A. Mercatanti, S. Hammond, G. Rainaldi, MicroRNAs modulate the angiogenic properties of HUVECs, Blood 108 (2006) 3068–3071.
[13] W.J. Yang, D.D. Yang, S. Na, G.E. Sandusky, Q. Zhang, G. Zhao, Dicer is required for embryonic angiogenesis during mouse development, J. Biol. Chem. 280 (2005) 9330–9335.
[14] R.C. Ryther, A.S. Flynt, J.A. Phillips 3rd, J.G. Patton, siRNA therapeutics: big potential from small RNAs, Gene Ther. 12 (2005) 5–11.
[15] N. Oku, Y. Yamazaki, M. Matsuura, M. Sugiyama, M. Hasegawa, M. Nango, A novel non-viral gene transfer system, polycation liposomes, Adv. Drug Deliv. Rev. 52 (2001) 209–218.
[16] S. Yamakawa, Y. Furuyama, N. Oku, Development of a simple cell invasion assay system, Biol. Pharm. Bull. 23 (2000) 1264–1266.
[17] N. Oku, T. Asai, K. Watanabe, K. Kuromi, M. Nagatsuka, K. Kurohane, H. Kikkawa, K. Ogino, M. Tanaka, D. Ishikawa, H. Tsukada, M. Momose, J. Nakayama, T. Taki, Anti-neovascular therapy using novel peptides homing to angiogenic vessels, Oncogene 21 (2002) 2662–2669.

International Journal of Pharmaceutics 362 (2008) 197–200

Contents lists available at ScienceDirect

International Journal of Pharmaceutics

journal homepage: www.elsevier.com/locate/ijpharm

Note

Particle size-dependent triggering of accelerated blood clearance phenomenon

Hiroyuki Koide[a], Tomohiro Asai[a], Kentaro Hatanaka[a], Takeo Urakami[a], Takayuki Ishii[a], Eriya Kenjo[a], Masamichi Nishihara[b], Masayuki Yokoyama[b], Tatsuhiro Ishida[c], Hiroshi Kiwada[c], Naoto Oku[a,*]

[a] *Department of Medical Biochemistry and Global COE Program, Graduate School of Pharmaceutical Sciences, University of Shizuoka, 52-1 Yada, Suruga-ku, Shizuoka 422-8526, Japan*
[b] *Kanagawa Academy of Science and Technology, KSP East 404, Sakado 3-2-1, Takatsu-ku, Kawasaki, Kanagawa 213-0012, Japan*
[c] *Department of Pharmacokinetics and Biopharmaceutics, Institute of Health Biosciences, The University of Tokushima, 1-78-1 Sho-machi, Tokushima 770-8505, Japan*

ARTICLE INFO

Article history:
Received 22 April 2008
Received in revised form 29 May 2008
Accepted 4 June 2008
Available online 7 June 2008

Keywords:
Polyethylene glycol
Liposomes
Accelerated blood clearance
Polymeric micelles
Nanocarriers

ABSTRACT

A repeat-injection of polyethylene glycol-modified liposomes (PEGylated liposomes) causes a rapid clearance of them from the blood circulation in certain cases that is referred to as the accelerated blood clearance (ABC) phenomenon. In the present study, we examined whether polymeric micelles trigger ABC phenomenon or not. As a preconditioning treatment, polymeric micelles (9.7, 31.5, or 50.2 nm in diameter) or PEGylated liposomes (119, 261 or 795 nm) were preadministered into BALB/c mice. Three days after the preadministration [^{3}H]-labeled PEGylated liposomes (127 nm) as a test dose were administered into the mice to determine the biodistribution of PEGylated liposomes. At 24 h after the test dose was given, accelerated clearance of PEGylated liposomes from the bloodstream and significant accumulation in the liver was observed in the mice preadministered with 50.2–795 nm nanoassemblies (PEGylated liposomes or polymeric micelles). In contrast, such phenomenon was not observed with 9.7–31.5 nm polymeric micelles. The enhanced blood clearance and hepatic uptake of the test dose (ABC phenomenon) were related to the size of triggering nanoassemblies. Our study provides important information for developing both drug and gene delivery systems by means of nanocarriers.

1. Introduction

PEGylated liposomes possessing a long-circulating characteristic have been widely used for delivery systems of both drugs and genes. PEG provides a steric barrier to nanocarriers for avoiding interaction with plasma proteins including opsonins and the cells of mononuclear phagocyte system (MPS) (Allen and Hansen, 1991; Sakakibara et al., 1996; Lasic, 1996). However, our recent reports demonstrated that the intravenous injection of PEGylated liposomes might significantly alter a pharmacokinetic behavior of them injected thereafter (Ishida et al., 2006a,c; Wang et al., 2007). A repeat-injection of PEGylated liposomes causes a rapid clearance of them from the blood circulation in certain cases. This phenomenon, referred to as the accelerated blood clearance (ABC) phenomenon, is considered to be related with anti-PEG IgM secretion from splenic B cells (Ishida et al., 2006a,c). Anti-PEG IgM, produced in response to an injected dose of PEGylated liposomes, selectively binds to them injected secondary (Wang et al., 2007).

However, the immune response against polymeric micelles was not known at all. Polymeric micelles are formed from block copolymers typically consisting of hydrophilic and hydrophobic polymer blocks (Kwon and Kataoka, 1995). They are of particular interest as a drug carrier because of their small particle sizes, efficiency in entrapping a satisfactory amount of hydrophobic drugs within the inner core, stability in the circulation, and their ability of sustained release of the drugs. Polymeric micelles were also considered as a less immune response carrier (Yokoyama et al., 1991; Gaucher et al., 2005).

In this study, we examined whether the preadministration of polymeric micelles possessing PEG chains alters the biodistribution of PEGylated liposomes or not. Moreover, we investigated the

Abbreviations: ABC phenomenon, accelerated blood clearance phenomenon; [^{3}H]-CHE, [^{3}H] cholesterylhexadecyl ether; MPEG-DSPE, 1,2-distearoyl-*sn*-glycero-3-phosphoethanolamine-*n*-[methoxy(polyethylene glycol)-2000]; MPS, mononuclear phagocyte system; PEG-PBLA, poly(ethylene glycol)-*b*-poly(β-benzyl L-aspartate); PEGylated liposomes, polyethylene glycol-modified liposomes.

* Corresponding author. Tel.: +81 54 264 5701; fax: +81 54 264 5705.
E-mail address: oku@u-shizuoka-ken.ac.jp (N. Oku).

0378-5173/$ – see front matter © 2008 Elsevier B.V. All rights reserved.
doi:10.1016/j.ijpharm.2008.06.004

particle size-dependency for triggering the phenomenon by use of PEGylated liposomes and polymeric micelles.

2. Materials and methods

2.1. Materials

Dipalmitoylphosphatidylcholine (DPPC), cholesterol and 1,2-distearoyl-*sn*-glycero-3-phosphoethanolamine-*n*-[methoxy(polyethylene glycol)-2000](MPEG-DSPE) were kindly gifted from Nippon Fine Chemical Co., Ltd. (Takasago, Hyogo, Japan). [^{3}H]cholesterylhexadecyl ether ([^{3}H]-CHE) was purchased from Amersham Pharmacia (Buckinghamshire, UK). All other reagents were analytical grade.

2.2. Animal

Five-week-old male BALB/c mice were purchased from Japan SLC Inc. (Shizuoka, Japan). The animals were cared for according to the animal facility guidelines of the University of Shizuoka. All animal experiments were approved by the Animal and Ethics Review Committee of the University of Shizuoka.

2.3. Preparation of polymeric micelles

Three block copolymers were used for polymeric micelle preparations. Their structures and compositions are summarized in Table 1. Poly (ethylene glycol)-*b*-poly(β-benzyl L-aspartate) (PEG-PBLA) was synthesized by polymerization of β-benzyl L-aspartate *N*-carboxy anhydride from an amino terminal of α-methyl-ω-aminopoly(oxyethylene), as reported previously (Yokoyama et al., 1992). Two partially esterified block copolymers, PEG-P(Asp(pentyl)) and PEG-P(Asp(nonyl)), were prepared by esterification of PEG-*b*-poly(aspartic acid) block copolymer by a reported method (Yamamoto et al., 2007). In brief, aspartic acid residues of PEG-*b*-poly(aspartic acid) block copolymer was activated with 1,8-diazabicyclo[5,4,0]7-undecene, followed by reaction with corresponding alkyl bromides, pentyl bromide and nonyl bromide.

Polymeric micelles were prepared from these three block copolymers by a dialysis method (Yamamoto et al., 2007). Block copolymers were dissolved in DMF at a concentration of 7.5 mg/ml. These polymer solutions were dialyzed against distilled water by the use of a dialysis membrane (Spectra/Por 6, molecular weight cut-off: 1000, Spectrum Japan, Tokyo, Japan). After overnight dialysis, the micelle solutions were concentrated by ultrafiltration (Millipore ultrafiltration membrane PBHK, molecular weight cut-off: 100,000, Nihon Millipore, Tokyo, Japan). By dynamic light scattering, weight-averaged diameters of the obtained polymeric micelles were found to be 50.2, 31.5, and 9.7 nm for PEG-PBLA, PEG-P(Asp(pentyl)), and PEG-P(Asp(nonyl)), respectively.

2.4. Preparation of PEGylated liposomes

PEGylated liposomes composed of DPPC and cholesterol with MPEG-DSPE (10:5:1 as molar ratio) were prepared as described previously (Maeda et al., 2004). In brief, lipids dissolved in chloroform were evaporated to form thin lipid film. Then liposomes were formed by hydration with 10 mM phosphate-buffered 0.3 M sucrose solution (pH 7.4). Then liposomes were sized by five times extrusion through a polycarbonate membrane filter with 100, 400 or 800 nm pores (Nucleopore, Maidstone, UK). For a biodistribution study, a trace amount of [^{3}H]-CHE (74 kBq/mouse) was added to the initial chloroform solution. Particle size of PEGylated liposomes diluted with PBS, pH 7.4, was measured by dynamic light scattering.

2.5. Biodistribution of PEGylated liposomes

Mice were received intravenous injection of polymeric micelles (2.9 mg/kg), PEGylated liposomes (2.0 μmol phospholipids/kg, 2.4 mg total lipids/kg) or phosphate-buffered sucrose. At three days later [^{3}H]-labeled test-dose PEGylated liposomes (5.0 μmol phospholipids/kg) were injected into them via a tail vein. Twenty-four hours after the test-dose administration, the mice were sacrificed for the collection of the blood from the carotid artery. Then the blood treated with heparin was centrifugally separated to obtain the plasma. After the blood was withdrawn, the heart, the lung, the liver, the spleen and the kidney were removed and weighed. The radioactivity in plasma and each organ was determined with a liquid scintillation counter (LSC-3100, Aloka, Tokyo, Japan). Distribution data are presented as % dose per wet tissue. The total amount in plasma was calculated based on the average body weight of the mice, where the average plasma volume was assumed to be 4.27% of the body weight based on the data on total blood volume.

2.6. Statistics

Variance in a group was evaluated by the *F*-test, and differences in biodistribution data, by Student's *t*-test.

3. Results and discussion

At first, we used PEGylated liposomes with 119, 261 or 795 nm diameter as a preconditioning dose. Fig. 1 shows the biodistribution of test-dose PEGylated liposomes (127 nm). The amount of the PEGylated liposomes in the plasma was significantly decreased and that in the liver was significantly increased in the mice preadministered with the PEGylated liposomes. ABC phenomenon was caused by all liposomes tested. Fig. 2 shows the biodistribution of test-dose PEGylated liposomes in the mice preadministered with polymeric micelles (9.7, 31.5 or 50.2 nm) at 3 days before. The mice prereceived

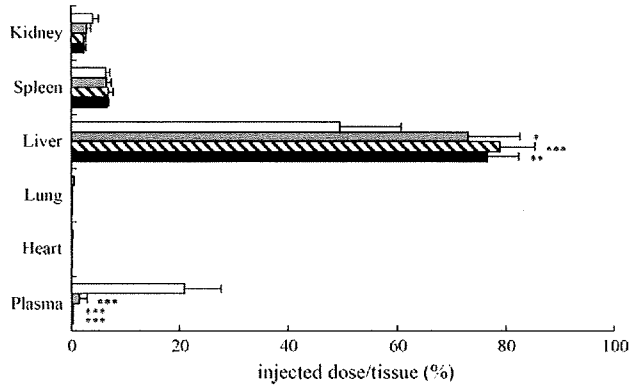

Fig. 1. Biodistribution of test-dose PEGylated liposomes after preadministration of various sized ones. BALB/c mice were intravenously injected with PEGylated liposomes (2.0 μmol phospholipids/kg) with 119, 261 or 795 nm size. Three days later [^{3}H]-labeled test-dose PEGylated liposomes (5.0 μmol phospholipids/kg) were administered via a tail vein. Twenty-four hours later, the mice were sacrificed and the radioactivity in the plasma and each organ was determined ($n = 5$). Data are presented as a percentage of the injected dose per tissue and S.D. Data represent phosphate-buffered sucrose (open bar), 119 nm (gray bar), 261 nm (hatched bar), and 795 nm (closed bar) PEGylated liposomes, respectively. Significant differences against phosphate-buffered sucrose group are shown with asterisks: $^*p < 0.05$; $^{**}p < 0.01$; $^{***}p < 0.001$.

Table 1
Composition of block copolymers

PEG-PBLA

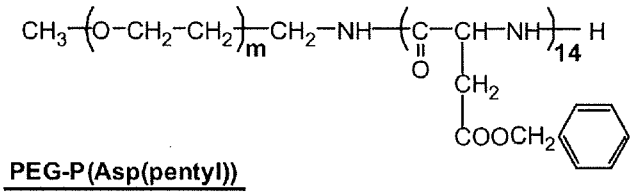

PEG-P(Asp(pentyl))
and PEG-P(Asp(nonyl))

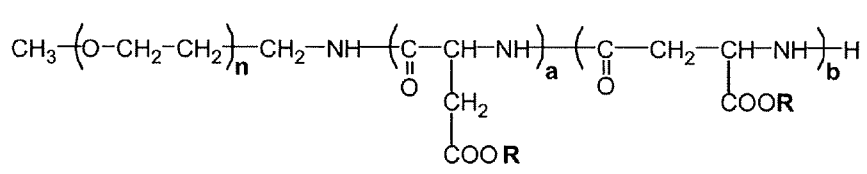

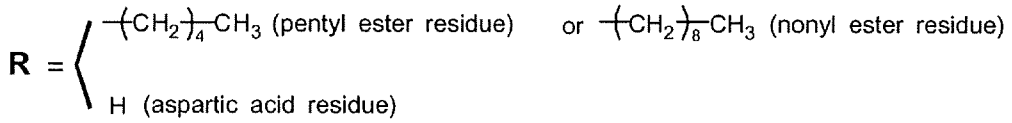

Copolymer	Molecular weight (M.W.)	M.W. of PEG block	Number of Asp units ($a+b$)	Esterification degree (%)[a]	Diameter (nm)[b]
PEG-PBLA	15,000	12,000	14	100	50.2
PEG-P(Asp(pentyl))	9,000	5,000	22	75	31.5
PEG-P(Asp(nonyl))	10,000	5,000	22	72	9.7

[a] Esterification degree (%) = (number of ester residues)/(number of ester residues) + (number of aspartic acid residues) × 100. This degree was determined by ^{1}H NMR measurements.

[b] Weight-weightened average diameter determined by dynamic light scattering.

50.2 nm polymeric micelles showed a significant decrease of test-dose PEGylated liposomes in the plasma and a significant increase in hepatic uptake. However, the preadministration of both 9.7 and 31.5 nm polymeric micelles did not change plasma concentration and hepatic uptake of test-dose PEGylated liposomes. It appears that ABC phenomenon was not caused by preadministration with smaller-sized polymeric micelles (31.5 nm or less), while it was triggered by preadministration with larger-sized polymeric micelles (50.2 nm or more). These results indicate that ABC phenomenon was triggered by preconditioning with not only PEGylated liposomes but also PEG-containing polymeric micelles. Furthermore, the size of nanoassemblies presenting PEG moiety on their surface is one of important factors to induce the ABC phenomenon. In case of large particles, they would be recognized easily by immune cells and activate immune systems, presumably in spleen (Ishida et al., 2006b). By contrast, small particles might avoid the recognition by immune cells. In the point of the molecular weight of PEG moiety, we previously reported that elongation of PEG chain length did not show any difference for inducing ABC phenomenon (Ishida et al., 2005). Consequently, the larger particles may produce anti-PEG IgM (Wang et al., 2007) that triggers enhanced blood clearance and hepatic uptake of test-dose PEGylated liposomes, although further investigation should be required to prove this assumption.

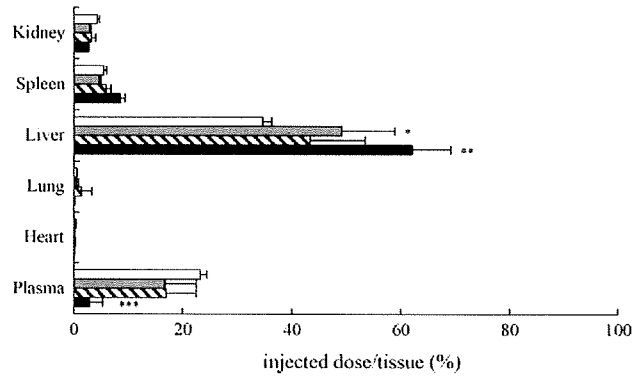

Fig. 2. Biodistribution of test-dose PEGylated liposomes after preadministration of various size polymeric micelles. BALB/c mice were intravenously injected with polymeric micelles (2.9 mg/kg) with 9.7, 31.5 or 50.2 nm size. Three days later [^{3}H]-labeled PEGylated test-dose liposomes (5.0 μmol phospholipids/kg) were administered via a tail vein. Twenty-four hours later, the mice were sacrificed and the radioactivity in the plasma and each organ was determined ($n=5$). Data are presented as a percentage of the injected dose per tissue and S.D. Data represent phosphate-buffered sucrose (open bar), 9.7 nm (gray bar), 31.5 nm (hatched bar), and 50.2 nm (closed bar) polymeric micelles, respectively. Significant differences against phosphate-buffered sucrose group are shown with asterisks: $^*p<0.05$; $^{**}p<0.01$; $^{***}p<0.001$.

4. Conclusions

This study is the first report to demonstrate that the preconditioning with polymeric micelles sized at around 50 nm, which are most widely used to deliver anti-cancer drug, causes the ABC phenomenon. Furthermore, it is clarified that the size of nanoassemblies is one of important factors for ABC phenomenon. Since nanocarriers are now progressing in the field of DDS, this study points out the important information about unexpected immune reactions against nanocarriers.

References

Allen, T.M., Hansen, C.B., 1991. Pharmacokinetics of stealth versus conventional liposomes: effect of dose. Biochim. Biophys. Acta 1068, 133–141.

Gaucher, G., Dufresne, M.H., Sant, V.P., Kang, N., Maysinger, D., Leroux, J.C., 2005. Block copolymer micelles: preparation, characterization and application in drug delivery. J. Control. Release 109, 169–188.

Ishida, T., Harada, M., Wang, X.Y., Ichihara, M., Irimura, K., Kiwada, H., 2005. Accelerated blood clearance of PEGylated liposomes following preceding liposome injection: effects of lipid dose and PEG surface-density and chain length of the first-dose liposomes. J. Control. Release 105, 305–317.

Ishida, T., Atobe, K., Wang, X., Kiwada, H., 2006a. Accelerated blood clearance of PEGylated liposomes upon repeated injections: effect of doxorubicin encapsulation and high-dose first injection. J. Control. Release 115, 251–258.

Ishida, T., Ichihara, M., Wang, X., Kiwada, H., 2006b. Spleen plays an important role in the induction of accelerated blood clearance of PEGylated liposomes. J. Control. Release 115, 243–250.

Ishida, T., Ichihara, M., Wang, X., Yamamoto, K., Kimura, J., Majima, E., Kiwada, H., 2006c. Injection of PEGylated liposomes in rats elicits PEG specific IgM, which is responsible for rapid elimination of a second dose of PEGylated liposomes. J. Control. Release 112, 15–25.

Kwon, G.S., Kataoka, K., 1995. Block copolymer micelles as long-circulating drug vehicles. Adv. Drug Deliv. Rev. 16, 295–301.

Lasic, D.D., 1996. Doxorubicin in sterically stabilized liposomes. Nature 380, 561–562.

Maeda, N., Takeuchi, Y., Takada, M., Sadzuka, Y., Namba, Y., Oku, N., 2004. Anti-neovascular therapy by use of tumor neovasculature-targeted long-circulating liposome. J. Control. Release 100, 41–52.

Sakakibara, T., Chen, F.A., Kida, H., Kunieda, K., Cuenca, R.E., Martin, F.A., Bankert, R.B., 1996. Doxorubicin encapsulated in sterically stabilized liposomes is superior to free drug or drug-containing conventional liposomes at suppressing growth and metastases of human lung tumor xenografts. Cancer Res. 56, 3743–3746.

Wang, X., Ishida, T., Kiwada, H., 2007. Anti-PEG IgM elicited by injection of liposomes is involved in the enhanced blood clearance of a subsequent dose of PEGylated liposomes. J. Control. Release 119, 236–244.

Yamamoto, T., Yokoyama, M., Opanasopit, P., Hayama, A., Kawano, K., Maitani, Y., 2007. What are determining factors for stable drug incorporation into polymeric micelle carriers? Consideration on physical and chemical characters of the micelle inner core. J. Control. Release 123, 11–18.

Yokoyama, M., Kwon, G.S., Okano, T., Sakurai, Y., Seto, T., Kataoka, K., 1992. Preparation of micelle-forming polymer–drug conjugates. Bioconjugate Chem. 3, 295–301.

Yokoyama, M., Okano, T., Sakurai, Y., Ekimoto, H., Shibazaki, C., Kataoka, K., 1991. Toxicity and antitumor activity against solid tumors of micelle-forming polymeric anticancer drug and its extremely long circulation in blood. Cancer Res. 51, 3229–3236.

JOURNAL OF BIOSCIENCE AND BIOENGINEERING
Vol. 106, No. 1, 99–102. 2008
DOI: 10.1263/jbb.106.99

In Vivo Protein Delivery to Human Liver-Derived Cells Using Hepatitis B Virus Envelope Pre-S Region

Takeshi Kasuya,[1] Tadanori Yamada,[1] Atsuko Uyeda,[1,2] Takashi Matsuzaki,[1,2] Toshihide Okajima,[1] Kenji Tatematsu,[1] Katsuyuki Tanizawa,[1,2] and Shun'ichi Kuroda[1,2]*

Department of Structural Molecular Biology, Institute of Scientific and Industrial Research, Osaka University, 8-1 Mihogaoka, Ibaraki, Osaka 567-0047, Japan[1] and Japan Science and Technology Agency (JST), 4-1-8 Honcho, Kawaguchi-shi, Saitama 332-0012, Japan[2]

Received 4 December 2007/Accepted 16 April 2008

Human hepatocyte-specific delivery of green fluorescent protein was succeeded in the mouse *xenograft* model by fusion with hepatitis B virus surface antigen pre-S regions (pre-S(1+2)), not with each pre-S region. The entire pre-S region would be useful for human liver-specific delivery of therapeutic proteins and bio-imaging fluoroproteins in biomedical field.

[**Key words:** hepatitis B virus, pre-S region, human liver, *in vivo* targeting, drug delivery system]

Several small peptides (up to 20 amino acids), when injected intravenously in animal models, have been shown to accumulate in specific tissues or organs by recognizing their blood vessels. These peptides are called homing peptides, and they are considered to be useful for tissue- or cancer-specific delivery of therapeutic compounds (1). However, a few homing peptides have succeeded in delivering large molecules *in vivo*, *e.g.*, tumor necrosis factor (TNF)α (2) and quantum dots (diameter 3–5 nm) (3). The delivery might have been possible because of a weak interaction between the homing peptides and the target organs and tissues, since the homing peptides were selected under artificial conditions (*i.e.*, using an *in vivo* panning method). Under natural conditions, various viruses have acquired their cell- and tissue-specificity (*i.e.*, tropism) during their evolution. The specificity of these viruses is usually determined by their surface proteins. The part of the surface proteins responsible for the cell- and tissue-specific delivery of a whole virus *in vivo* is considered to be useful as a targeting molecule for large molecules.

Hepatitis B virus (HBV) infects liver cells specifically in human and chimpanzee, not those in other animals. The hepatophilicity is determined by the pre-S regions (pre-S(1+2); pre-S1, 119 amino acid residues (aa) in HBV subtype *adr*; pre-S2, 55 aa) at the N-terminal half of HBV surface antigen (HBsAg) L protein (4). Further studies showed that pre-S1 [21–47] is indispensable for the specific binding of HBV to hepatocytes (5) and pre-S2 [41–52] is necessary for both poly-albumin-mediated cell attachment of HBV (6) and cell permeable ability of HBV (7, 8). In this study, we investigated whether the pre-S region can transport green fluorescent protein (GFP) to transplanted tumors in a mouse *xenograft* model. The results shown here will facilitate the use of viral surface proteins as an efficient *in vivo* targeting molecule in biomedical field (*e.g.*, drug delivery system, bio-imaging).

DNA fragments encoding pre-S proteins (pre-S1, pre-S2, pre-S(1+2)) were inserted into the pGEX-6p-GFP plasmid (GE, Piscataway, NJ, USA) to express the N-terminally GST (glutathione *S*-transferase)-GFP-fused pre-S proteins in *E. coli* BL21 (Fig. 1A). The transformant harboring each plasmid was cultured, and the crude lysate was subjected to the glutathione-coupled Sepharose column. The GFP-pre-S proteins (GFP-pre-S1, GFP-pre-S2, GFP-pre-S(1+2)) were eluted by digestion with PreScission proteinase (GE). Approximately 1.5 mg of GFP-pre-S protein was obtained from each transformant grown in 1 *l* broth. These GFP-pre-S proteins were confirmed more than 95% purity by SDS–PAGE analysis followed by CBB staining (Fig. 1B). The molecular mass of each GFP-pre-S protein coincided well with the mo-

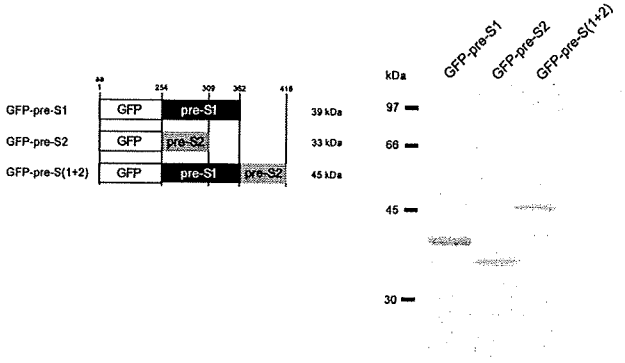

FIG. 1. Production of N-terminally GFP-fused pre-S proteins. (A) GFP-pre-S1, GFP-pre-S2, and GFP-pre-S(1+2) proteins. Amino acid residues (aa) are indicated in the upper margin. (B) The purified GFP-pre-S protein was analyzed with SDS–PAGE followed by CBB R-250 staining.

* Corresponding author. e-mail: skuroda@sanken.osaka-u.ac.jp
phone/fax: +81-(0)6-6879-8462

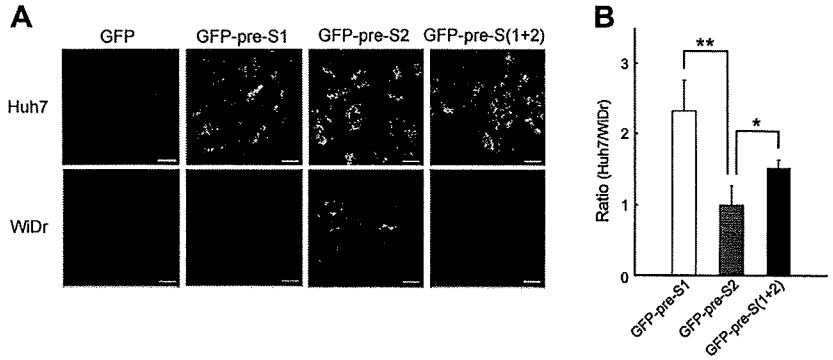

FIG. 2. Accumulation of GFP-pre-S proteins in cultured cells (*in vitro*). (A) About 2.5×10^5 cells of Huh7 and WiDr grown on a 3.5-cm glass-bottom dish were mixed with 30 μg of GFP-pre-S proteins, and then incubated for 6 h, fixed with 2% (w/v) paraformaldehyde, washed with PBS twice, and then observed under a LSM5 Pascal confocal laser microscope (Carl Zeiss, Oberkochen, Germany). Scale bars: 10 μm. (B) Ratio of the relative fluorescent unit (RFU) derived from GFP-pre-S proteins in Huh7 to that in WiDr cells. RFU was calculated from the TIFF files taken under the same conditions. Ten cells in the same visual field were analyzed with NIH image J software (Bethesda, MA, USA). n=7; mean±s.d.; * <0.05 and ** <0.001, *t*-test.

lecular weight calculated from each amino acid sequence.

We added 30 μg GFP-pre-S proteins to human hepatocellular carcinoma Huh7 cells and human colon adenocarcinoma WiDr cells. The fluorescent intensity of each cell was determined from the images with NIH image software. When either GFP-pre-S1 or GFP-pre-S(1+2) was applied, the GFP-derived fluorescence was observed only in Huh7 cells, while GFP alone produced no fluorescence in any cell (Fig. 2A). Comparing the fluorescence derived from GFP-pre-S1, GFP-pre-S2, or GFP-pre-S(1+2) in Huh7 cells with that in WiDr cells (Fig. 2B), both pre-S1 and pre-S(1+2) regions were revealed to possess enough activity for the *in vitro* targeting of human liver-derived cells. Intriguingly, GFP-pre-S2 produced fluorescence in both cells. Since the pre-S2 [41–52] region is a translocation motif (TLM) showing an energy-independent cell-permeable ability (7, 8), the GFP-pre-S2 might have the ability to penetrate into every type of cell.

When the intracellular localization of GFP-pre-S(1+2) in Huh7 cells was investigated by an immunocytochemical method using DAPI (4′,6-diamidino-2-phenylindole), the protein was found to accumulate as dots around the nucleus (Fig. 3, upper panels). Next, since Lamp-2 (late endosome-associated protein-2) protein localizes in the lysosomes and late endosomes in the perinuclear region, the cells were stained with anti-Lamp-2 antibody (Fig. 3, lower panels). A part of GFP-pre-S(1+2) was found to co-localize with Lamp-2 as dots, suggesting that GFP-pre-S(1+2) is incorporated not by membrane fusion but by endocytosis and is finally sorted to either the late endosome or lysosome.

We injected 300 μg of GFP-pre-S proteins intravenously into the tail vein of *xenograft* model mice harboring human hepatocellular carcinoma NuE- and WiDr-derived tumors. Sixteen hours after the injection, both tumors and tissues were isolated and embedded in synthetic resin. Slices of 5-μm width were analyzed under a laser scanning confocal microscope. As shown in Fig. 4A, green fluorescence was detected in the NuE-derived tumors of the mice administrated with GFP-pre-S(1+2). Neither fluorescence was observed in WiDr-derived tumors, brains, hearts, lungs, livers, spleens nor kidneys (Fig. 4B), nor was fluorescence observed in the same tissues of the mice administrated with

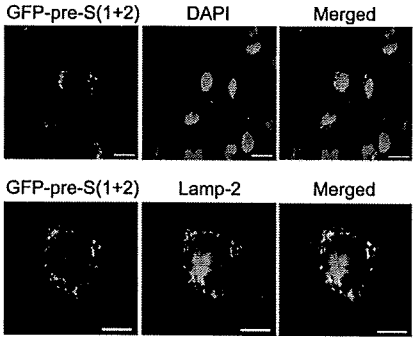

FIG. 3. Intracellular localization of GFP-pre-S(1+2) in Huh7 cells (*in vitro*). After the cells were treated with GFP-pre-S(1+2) for 6 h, the nuclei were stained with DAPI and observed under a fluorescent microscope IX-70 (Olympus, Tokyo) (upper panels). For immunocytochemical observation, the permeabilized cells were reacted with the anti-Lamp-2 monoclonal antibody (dilution factor 1000, clone H4B4; DSHB, Iowa City, IA, USA) overnight at 4°C, and then with the Cy3-conjugated anti-mouse IgG (dilution factor 1000; Jackson ImmunoResearch Laboratories, West Baltimore Pike, PA, USA) at room temperature for 30 min. The fluorescence was visualized under a laser scanning confocal microscope (lower panels). Scale bars: 10 μm.

GFP-pre-S1, GFP-pre-S2, or GFP (data not shown). These data agreed well with the hepatophilic property of HBV (only to human and chimpanzee, not to other animals) (4).

After infection, various viruses are circulated in the body and then sorted to target tissues *in vivo* by the action of their surface proteins, implying that the affinity of surface proteins to target tissues is sufficient to allow the pinpoint delivery of large molecules in the body, even nano-sized virions. Considering the homing peptide as an *in vivo* transporter of large molecules, only a few homing peptides have succeeded in making the delivery to specific tissues *in vivo*, such as TNFα and quantum dots (2, 3). The action of homing peptides has often been restrained by the conjugation of large molecules, which has restricted us to using homing peptides for the delivery of small molecules (*e.g.*, peptides, chemical compounds) (9, 10). In this study, the systemic injection of GFP-pre-S(1+2) allowed the specific accumulation of GFP-derived fluorescence in the human hepatocyte-derived tumors

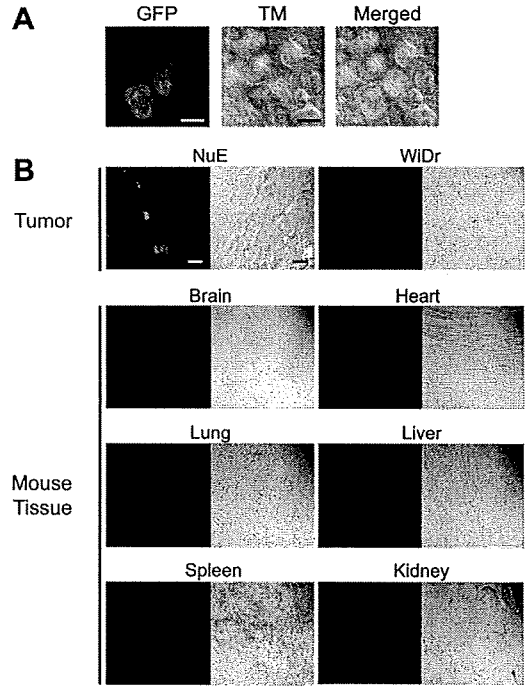

FIG. 4. Accumulation of GFP-pre-S(1+2) in the mouse *xenograft* tumor. BALB/c-nu/nu nude mice (8–9 weeks old, male; CLEA, Tokyo) bearing tumors (about 1 cm in diameter) derived from NuE and WiDr received an intravenous injection of 300 μg of GFP-pre-S proteins via the tail vein. Sixteen hours after the injection, these mice were anesthetized, followed by heart perfusion with PBS and then with 4% paraformaldehyde. Mouse brains, hearts, lungs, livers, spleens, kidneys and tumors were isolated and fixed in 4% paraformaldehyde for 1 night at 4°C. Tissues were embedded in synthetic resin with Technovit 8100 (Kulzer, Wehrheim, Germany). Sections at a width of 5 μm were prepared from resin blocks and observed under a laser scanning confocal microscope. TM, Transmission image. Scale bars: 10 μm.

in the mouse *xenograft* model (see Fig. 4). This is the first demonstration that the pre-S region functions as a targeting molecule for large molecules to permeate human hepatocytes *in vivo*, which would prompt us to examine surface proteins derived from other viruses as targeting molecules for the *in vivo* pinpoint delivery system, for example, HCV (hepatitis C virus) for the liver and JEV (Japanese encephalitis virus) and rabies virus for the brain. The pre-S(1+2) region may facilitate the human liver-specific delivery of therapeutic proteins (*e.g.*, interferons for the treatment of hepatitis B, hepatitis C, and malaria). As shown in Fig. 3, GFP-pre-S(1+2) was incorporated by Huh7 cells, followed by localization in the Lamp-2-containing organelles, late endosomes, or lysosomes. Generally, the materials localized in late endosomes are sorted to lysosomes for degradation. The incorporated GFP-pre-S(1+2) would be processed by the lysosomal protein degradation system, which may be an obstacle for the practical application of pre-S(1+2) in a drug delivery system (DDS).

Recently, herpes simplex virus type 1, originally infecting various cell types by the binding of its glycoproteins (gp) B and C to cell surface glycosaminoglycans, has been retargeted toward human hepatocytes *in vitro* by substitution of the HBV pre-S1 region for the glycosaminoglycan-binding domain of gpC (11). On the other hand, the pre-S2 region is considered to mediate the cell permeability of HBV (6, 7). In this study, both pre-S1 and pre-S2 were shown to contribute synergistically to the human liver-specific delivery of large molecules *in vivo*, though neither pre-S1 nor pre-S2 was sufficient for the *in vivo* delivery. These data suggested that pre-S1 and pre-S2 are prerequisite to the attachment to the cell surface and the penetration into cells, respectively, for not only GFP-pre-S(1+2) but also HBV.

We have previously demonstrated that the L particle consisting of HBsAg L proteins is capable of delivering incorporated materials to human hepatocytes *in vitro* and *in vivo* (12). The L particle was able to deliver fluorescent dye to human liver-derived cells (including Huh7 and NuE) exclusively and not to control cells (including WiDr), unlike GFP-pre-S(1+2), as shown in Figs. 2A and 2B. These results strongly suggested that the hepatophilic property of L particle is significantly higher than that of pre-S(1+2). Previous research showed that the S region contained in L particle and HBV interacts with cellular endocytosis-related proteins (13, 14) and includes a membrane-fusion peptide (15), and both functions are considered to play pivotal roles in the cellular entry of HBV. Thus, the precise liver-specificity of HBV and L particle as regards cellular attachment and entry may be achieved by the synergistic action of pre-S1, pre-S2, and S regions. However, the S region links antigenic loops by inter- and intra-molecular disulfide bonds, and forms high-molecular-weight multiprotein complexes. When applying L particle as a DDS carrier in humans, undesired immune responses may be inevitable due to the multiple complexes of HBsAg (16). From the viewpoint of immunogenicity, the pre-S(1+2) region, much smaller than L particle, could be more advantageous for the administration of therapeutic proteins in humans.

The authors thank Prof. T. Tadakuma (National Defense Medical College) and Prof. M. Ueda (Keio University) for providing NuE cell, and Prof. Y. Wada (Osaka University) for helpful discussion. This work was supported in part by the Scientific Research on Priority Areas (no. 18015032) from the Ministry of Education, Culture, Sports, Science and Technology of Japan, "Creation of biodevices and bio-systems with chemical and biological molecules for medical use (CREST)", the Regional Research and Development Resources Utilization Program from the Japan Science and Technology Agency (JST), and the Grants-in-Aid for Research on Advanced Medical Technology from the Ministry of Health, Labour and Welfare.

REFERENCES

1. **Kolonin, M., Pasqualini, R., and Arap, W.:** Molecular addresses in blood vessels as targets for therapy. Curr. Opin. Chem. Biol., **5**, 308–313 (2001)
2. **Curnis, F., Sacchi, A., Borgna, L., Magni, F., Gasparri, A., and Corti, A.:** Enhancement of tumor necrosis factor alpha antitumor immunotherapeutic properties by targeted delivery to aminopeptidase N (CD13). Nat. Biotechnol., **18**, 1185–1190 (2000).
3. **Akerman, M. E., Chan, W. C., Laakkonen, P., Bhatia, S. N., and Ruoslahti, E.:** Nanocrystal targeting in vivo. Proc. Natl. Acad. Sci. USA, **99**, 12617–12621 (2002).
4. **Neurath, A. R., Kent, S. B., Strick, N., and Parker, K.:** Identification and chemical synthesis of a host cell receptor

binding site on hepatitis B virus. Cell, **46**, 429–436 (1986).
5. **Le Seyec, J., Chouteau, P., Cannie, I., Guguen-Guillouzo, C., and Gripon, P.:** Infection process of the hepatitis B virus depends on the presence of a defined sequence in the pre-S1 domain. J. Virol., **73**, 2052–2057 (1999).
6. **Itoh, Y., Kuroda, S., Miyazaki, T., Otaka, S., and Fujisawa, Y.:** Identification of polymerized-albumin receptor domain in the pre-S2 region of hepatitis B virus surface antigen M protein. J. Biotechnol., **23**, 71–82 (1992).
7. **Oess, S. and Hildt, E.:** Novel cell permeable motif derived from the PreS2-domain of hepatitis-B virus surface antigens. Gene Ther., **7**, 750–758 (2000).
8. **Stoeckl, L., Funk, A., Kopitzki, A., Brandenburg, B., Oess, S., Will, H., Sirma, H., and Hildt, E.:** Identification of a structural motif crucial for infectivity of hepatitis B viruses. Proc. Natl. Acad. Sci. USA, **103**, 6730–6734 (2006).
9. **Arap, W., Pasqualini, R., and Ruoslahti, E.:** Cancer treatment by targeted drug delivery to tumor vasculature in a mouse model. Science, **279**, 377–380 (1998).
10. **Laakkonen, P., Akerman, M. E., Biliran, H., Yang, M., Ferrer, F., Karpanen, T., Hoffman, R. M., and Ruoslahti, E.:** Antitumor activity of a homing peptide that targets tumor lymphatics and tumor cells. Proc. Natl. Acad. Sci. USA, **101**, 9381–9386 (2004).
11. **Argnani, R., Boccafogli, L., Marconi, P. C., and Manservigi, R.:** Specific targeted binding of herpes simplex virus type 1 to hepatocytes via the human hepatitis B virus preS1 peptide. Gene Ther., **11**, 1087–1098 (2004).
12. **Yamada, T., Iwasaki, Y., Tada, H., Iwabuki, H., Chuah, M. K., VandenDriessche, T., Fukuda, H., Kondo, A., Ueda, M., Seno, M., Tanizawa, K., and Kuroda, S.:** Nanoparticles for the delivery of genes and drugs to human hepatocytes. Nat. Biotechnol., **21**, 885–890 (2003).
13. **De Meyer, S., Depla, E., Maertens, G., Soumillion, A., and Yap, S. H.:** Characterization of small hepatitis B surface antigen epitopes involved in binding to human annexin V. J. Viral Hepat., **6**, 277–285 (1999).
14. **Mehdi, H., Kaplan, M. J., Anlar, F. Y., Yang, X., Bayer, R., Sutherland, K., and Peeples, M. E.:** Hepatitis B virus surface antigen binds to apolipoprotein H. J. Virol., **68**, 2415–2424 (1994).
15. **Berting, A., Fischer, C., Schaefer, S., Garten, W., Klenk, H. D., and Gerlich, W. H.:** Hemifusion activity of a chimeric influenza virus hemagglutinin with a putative fusion peptide from hepatitis B virus. Virus Res., **68**, 35–49 (2000).
16. **Lawrence, D.:** Nanotechnology takes another small step forward. Lancet, **362**, 48 (2003).

HUMAN GENE THERAPY 19:887–895 (September 2008)

DOI: 10.1089/hum.2008.037

In Vivo Delivery of Bionanocapsules Displaying *Phaseolus vulgaris* Agglutinin-L_4 Isolectin to Malignant Tumors Overexpressing *N*-Acetylglucosaminyltransferase V

Takeshi Kasuya,[1] Joohee Jung,[1,2] Hiroyasu Kadoya,[1] Takashi Matsuzaki,[1,2] Kenji Tatematsu,[1] Toshihide Okajima,[1] Eiji Miyoshi,[3] Katsuyuki Tanizawa,[1,2] and Shun'ichi Kuroda[1,2]

Abstract

Metastasis is a key aspect of tumor malignancy, and several malignant tumors show expression of various mature N-type glycans. In particular, β1-6 branching *N*-acetylglucosamine (GlcNAc) is abundantly expressed as a part of high-mannose glycans in various highly metastatic cancers. *Phaseolus vulgaris* agglutinin-L_4 isolectin (L_4-PHA), which adheres to β1-6 GlcNAc specifically, has been used for *in situ* cancer diagnosis. Bionanocapsules (BNCs), hollow particles with a diameter of approximately 80 nm and composed of hepatitis B surface antigen (HBsAg) and a lipid bilayer, have been developed as human liver-specific nanocapsules for *in vivo* drug delivery system. In this study, we have generated L_4-PHA-displaying BNCs (PHA–BNCs) and examined whether L_4-PHA could retarget the BNCs to malignant tumors as a "biosensor" distinguishing tumor metastaticity. Fluorescence-labeled PHA–BNCs injected systemically into a mouse xenograft model were found to accumulate in β1-6 GlcNAc-expressing malignant tumors. The PHA–BNCs were able to deliver DNA to the malignant cancer cells. These results open up the possibility of using L_4-PHA lectin as a targeting molecule in a drug delivery system, and of using PHA–BNCs as a novel nanodevice for malignant tumor-specific bioimaging and drug delivery.

Introduction

ABERRANT EXPRESSION of various glycans on the surface of tumors is associated with many pathophysiological events during tumor progression, such as adhesion, proliferation, migration, apoptosis suppression, and metastasis (Hakomori, 1989). The presence on the surface of tumors of β1-6 branching *N*-acetylglucosamine (GlcNAc), which has been studied for decades, is associated with malignant transformation of rodent and human cells, and poor prognosis in cancer patients (Dennis *et al.*, 1999). Either tri- or tetraantennary *N*-glycans are synthesized with *N*-acetylglucosaminyltransferase V (GnT-V) by transferring β1-6 branching GlcNAc to the trimannosyl core (Yamashita *et al.*, 1985). GnT-V activity is upregulated by overexpression of proto-oncogenes (Buckhaults *et al.*, 1997; Chen *et al.*, 1998; Ko *et al.*, 1999), and the overexpression of GnT-V in cancer cell lines has enhanced metastasis in animal models (Ihara *et al.*, 2002; Murata *et al.*, 2004). Metastatic tumor tissues excised from patients (e.g., colon cancer, breast cancer, melanoma, and lung cancer) have shown higher expression of GnT-V and increased amount of β1-6 GlcNAc (Fernandes *et al.*, 1991; Murata *et al.*, 2000; Handerson and Pawelek, 2003; Dosaka-Akita *et al.*, 2004). Moreover, polyoma virus middle T antigen-induced breast tumors in *GnT-V* gene-deficient mice are much smaller than those in wild-type mice, and have shown a low incidence of metastasis (Granovsky *et al.*, 2000; Dennis *et al.*, 2002). These results have indicated that β1-6 GlcNAc in *N*-glycans plays crucial roles in both tumor progression and metastasis.

Some plant-derived lectins have been revealed by *in vitro* and *in vivo* studies to possess antitumor activity (Wimer, 1990; Abdullaev and De Mejia, 1997), although how lectins exhibit therapeutic effects has remained unsettled on a mo-

[1]Department of Structural Molecular Biology, Institute of Scientific and Industrial Research, Osaka University, Ibaraki, Osaka 567-0047, Japan.
[2]Japan Science and Technology Agency, Kawaguchi, Saitama 332-0012, Japan.
[3]Department of Molecular Biochemistry and Clinical Investigation, Graduate School of Medicine, Osaka University, Osaka 565-0871, Japan.

lecular basis. In particular, the kidney bean-derived lectin, *Phaseolus vulgaris* agglutinin-L_4 (L_4-PHA), has been administered intravenously to cancer patients, and has shown a weak therapeutic effect without severe side effects (Wimer, 1997). L_4-PHA has been used for cancer diagnosis, specifically *in situ* histological analysis to identify β1-6 GlcNAc-expressing malignant cancer cells (Cumming and Kornfeld, 1982; Raedler and Shreiber, 1988). These applications strongly suggest that L_4-PHA possesses both sufficient safety in cancer patients and high affinity for malignant tumors, and led us to examine whether L_4-PHA is capable of delivering drug delivery system (DDS) carriers to malignant tumors *in vivo* by systemic administration.

A bionanocapsule (BNC) is a hollow particle about 80 nm in diameter and composed of about 130 molecules of hepatitis B virus (HBV) surface antigen (HBsAg) L proteins and a lipid bilayer (Kuroda *et al.*, 1992; Yamada *et al.*, 2001). The N-terminal outer membrane region (pre-S region) of HBsAg is indispensable for the attachment of HBV to human liver cells (Neurath *et al.*, 1986), and the C-terminal transmembrane region (S), including a membrane-fusion peptide sequence (Berting *et al.*, 2000), interacts with cellular endocytosis-related proteins (Mehdi *et al.*, 1994; De Meyer *et al.*, 1999). These regions are postulated to contribute concurrently to human liver-specific infection with HBV. Various materials (e.g., DNA, chemicals, and polystyrene beads) can be incorporated by either electroporation (Yamada *et al.*, 2003; Iwasaki *et al.*, 2007) or liposome conjugation (Jung *et al.*, 2008). Intravenous injection of BNCs has allowed the efficient delivery of incorporated payloads to human liver-derived cells and tumors by using the HBV infection machinery (Yamada *et al.*, 2003; Iwasaki *et al.*, 2007; Jung *et al.*, 2008). The cell and tissue specificity of BNCs can be altered by replacing the pre-S region with other targeting molecules: for example, epidemical growth factor (EGF) for EGFR (EGF receptor)-expressing cells (Yamada *et al.*, 2003), and anti-EGFR antibody for EGFR-expressing tumors (Tsutsui *et al.*, 2007). Thus, BNCs have facilitated the *in vivo* pinpoint delivery of various materials to cells and tissues of interest.

In this study, we have generated L_4-PHA-displaying BNCs (PHA–BNCs) by means of the avidin–biotin conjugation system to target malignant cancer cells (GnT-V-overexpressing cells) in cultured cells (*ex vivo*) and a mouse xenograft model (*in vivo*).

Materials and Methods

Preparation of L_4-PHA-displaying BNCs

The BNC-harboring HBsAg mutant, the pre-S region of which was replaced with an IgG Fc-binding motif derived from *Staphylococcus aureus* protein A (Tsutsui *et al.*, 2007), was produced as described previously (Yamada *et al.*, 2003). Purified BNCs were biotinylated with sulfonated *N*-hydroxysulfosuccinimide (NHS)–biotin (Pierce Biotechnology, Rockford, IL). Biotinylated BNCs (bio-BNCs) were purified with a Zeba desalt spin column (Pierce Biotechnology). Biotinylated lectin (*Phaseolus vulgaris* agglutinin-L_4; L_4-PHA) obtained from Seikagaku (Tokyo, Japan), was mixed with an equimolar amount of streptavidin (SA; Seikagaku) and incubated for 10 min at room temperature to produce SA-conjugated PHA (SA–PHA) complex. The complex was mixed with an equimolar amount of bio-BNCs (as HBsAg protein) for 30 min at room temperature to produce L_4-PHA lectin-displaying BNCs (PHA–BNCs).

Quartz crystal microbalance analysis and size measurement of PHA–BNCs

The weight of protein displayed on the BNC surface was quantitated by quartz crystal microbalance (QCM) at 25°C, using a Twin-Q (As One Corp., Osaka, Japan), which has two 500-μl cells equipped with 27-MHz QCM plates. Bio-BNCs (about 100 ng as HBsAg protein) were immobilized on a gold electrode, and the electrode was washed and blocked with skim milk at a final concentration of 0.04% (w/v). The adsorption of SA onto bio-BNCs and the additional absorption of bio-PHA onto SA–BNCs were monitored by frequency change, with 1 Hz corresponding to 30 pg of absorbed protein. The size distribution and average size of PHA–BNCs were determined in phosphate-buffered saline (PBS) at 25°C by dynamic light scattering, using a Zetasizer model Nano-ZS (Malvern Instruments, Worcestershire, UK). The polydispersity index (PDI) is a width parameter for z-average as an intensity mean.

Immunoprecipitation

PHA–BNCs (20 μg as HBsAg protein) was incubated for 5 min at room temperature with 1 ml of PBS containing 5% (w/v) bovine serum albumin (BSA) and 0.01% (v/v) Triton X-100, mixed with mouse monoclonal anti-S region IgG-conjugated microbeads (20 μl, 50% [v/v] slurry) supplied as the IMx HBsAg assay system (Abbott Japan, Tokyo, Japan), and incubated for 5 min at room temperature. The microbeads were washed three times with PBS containing 5% BSA and 0.01% Triton X-100, boiled in Laemmli sample buffer for 15 min, and analyzed by Western blotting with horseradish peroxidase-conjugated SA (HRP–SA; GE Healthcare, Giles, Buckinghamshire, UK) and the enhanced chemiluminescence method (ECL Plus; GE Healthcare).

Cells

The human colon adenocarcinoma cell line WiDr and the human gastric cancer cell line MKN45 were cultured in Dulbecco's minimal essential medium (DMEM) supplemented with 10% (v/v) fetal bovine serum (FBS). GnT-V-expressing stable cell lines, WiDr-GnT-V (Murata *et al.*, 2004) and MKN45-GnT-V (Ihara *et al.*, 2002), were cultured in the same medium containing G418 (300 μg/ml; Nakalai Tesque, Kyoto, Japan).

Lectin blotting

Cells were lysed with 50 m*M* Tris-HCl (pH 8.0) containing 1 m*M* EDTA, 1 m*M* dithiothreitol, and 1% (v/v) Triton X-100. A blot containing 10 μg of lysate (as protein) in each lane was blocked overnight at 4°C with PBS containing 3% (w/v) BSA, incubated with bio-PHA (1 μg/ml) for 1 hr at room temperature, washed three times with PBS containing 0.01% Triton X-100, and then visualized with HRP–SA and ECL Plus.

Cytochemical analysis with L_4-PHA lectin

Cells (about 1×10^5) were cultured on a 24-well plate (BD Biosciences, San Jose, CA) for 24 hr, washed twice with ice-

cold PBS, and kept on ice in complete medium containing bio-PHA (1 μg/ml) for 1 hr. Cells were washed twice with ice-cold PBS, fixed with 4% (w/v) paraformaldehyde in PBS for 15 min at room temperature, stained with Alexa 488-labeled SA (0.2 μg/ml; Invitrogen, Carlsbad, CA) and Hoechst 33342 (2.5 μg/ml) for 1 hr at room temperature, washed three times with PBS, and then observed under a confocal laser microscope (FV-1000D; Olympus, Tokyo, Japan).

Ex vivo *delivery of PHA–BNCs*

Bio-BNCs were labeled with a membrane probe, 1,1′-dioctadecyl-3,3,3′,3′-tetramethylindodicarbocyanine, 4-chlorobenzenesulfonate (DiD; Invitrogen) (excitation at 644 nm, emission at 665 nm), passed through a Zeba desalt spin column, and then conjugated with SA–PHA. Cells (about 1×10^5) were cultured on a 24-well plate for 24 hr and incubated with DiD-labeled PHA–BNCs (5 μg as HBsAg protein) for 3 hr in complete medium. Delivery of PHA–BNCs was observed as described above. For flow cytometric analysis, the cells incubated with DiD-labeled PHA–BNCs were washed with PBS, treated with 0.25% (w/v) trypsin–EDTA for 15 min at 37°C, and washed with ice-cold PBS three times. The cells were analyzed with a FACSCanto II (BD Biosciences) equipped with 633-nm excitation laser and 660-nm long-path filter. Thirty thousand cells were counted in each sample. The obtained data were analyzed with FlowJo software (Tree Star, Ashland, OR).

In vivo *optical imaging*

All animal experiments were approved by the committee for experimental animal science of the Institute of Scientific and Industrial Research (Osaka University, Osaka, Japan). Animals were treated according to the guidelines of the Ministry of Education, Culture, Sports, Science, and Technology, Japan. Either WiDr-GnT-V cells or WiDr cells (about 1×10^5) were suspended in 100 μl of DMEM containing 10% (v/v) BD Matrigel matrix HC (BD Biosciences) and injected subcutaneously into the backs of BALB/c (*nu/nu*) nude mice (5 weeks old, male; CLEA, Tokyo, Japan). When tumors reached about 1 cm in diameter, DiD-labeled PHA–BNCs (40 μg as HBsAg protein) were injected through the tail vain. One, 4, 8, 16, 24, and 48 hr after injection, whole-body fluorescence was observed with an *in vivo* optical imaging system (OV100; Olympus). Twenty-four hours after injection, the mice were killed; livers, hearts, and tumors were isolated surgically, and their fluorescence was observed similarly. Fluorescence intensity was analyzed with Wasabi software (Hamamatsu Photonics, Hamamatsu, Japan). The number of mice in each group was three.

Ex vivo *gene delivery*

Incorporation of DNA into BNCs was performed by the BNC–liposome complex method (Jung *et al.*, 2008). Briefly, a freeze-dried form of cationic liposomes (1.5 mg as lipids; Coatsome EL-01-D; NOF, Tokyo, Japan) was mixed with firefly-derived luciferase expression vector pGL3 (250 μg; Promega, Madison, WI) to form the lipoplex (liposome–DNA complex). Aliquots (100 μg of liposomes, 16.7 μg of DNA) were incubated with bio-BNCs (100 μg as HBsAg protein) for 30 min at room temperature to allow the formation of a BNC–liposome–DNA complex. About 1×10^5 cells in a 24-well plate were incubated with the complex (1 μg as HBsAg protein) for 3 hr and cultured in fresh complete medium for 72 hr; and then the luciferase activity of each cell lysate was measured with a luciferase assay system (Promega).

Results

Preparation of BNCs displaying L_4-PHA lectin

Purified BNCs were biotinylated with sulfonated NHS–biotin, and conjugated with SA-conjugated L_4-PHA (SA–PHA) to produce L_4-PHA-displaying BNCs (PHA–BNCs). The amount of protein displayed on the bio-BNC surface was measured with a quartz crystal microbalance (QCM). On the basis of the change in oscillation frequency of the quartz crystal, the amount of SA displayed on 1 mol of BNCs was calculated as 35.6 mol. Because the number of HBsAg molecules embedded in the BNC lipid bilayer is about 130 (M. Iijima and S. Kuroda, unpublished observations; *see* Yamada *et al.*, 2001), 1 mol of HBsAg was estimated to bind with 0.32 mol of SA. Similarly, 5.7 mol of bio-PHA was estimated to bind with 1 mol of SA–BNCs. Next, the average sizes of bio-BNCs, SA–BNCs, and PHA–BNCs were determined by dy-

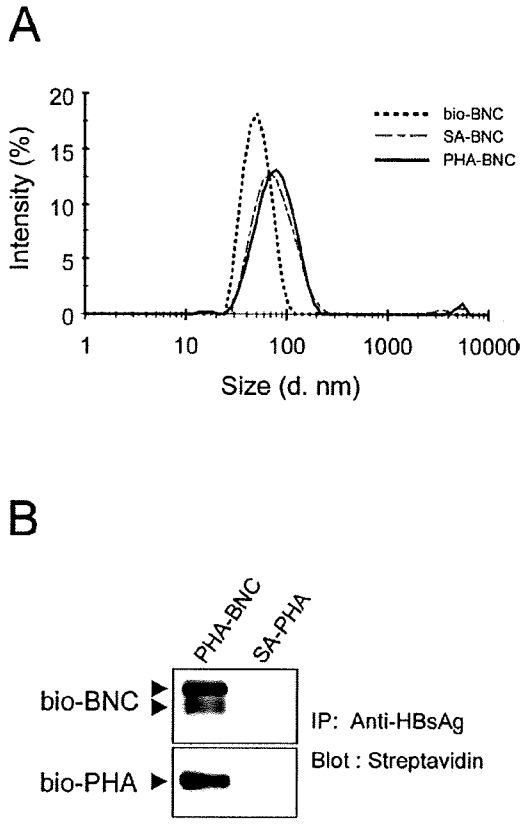

FIG. 1. Preparation of PHA–BNCs. (**A**) The diameters (nm) of bio-BNCs (dotted line), SA–BNCs (dashed line), and PHA–BNCs (solid line) were measured by dynamic light scattering (3 batches, 12 measurements for each batch). (**B**) PHA–BNCs and SA–PHA (negative control) were immunoprecipitated with an anti-HBsAg antibody, and analyzed by Western blotting with HRP–SA.

namic light scattering as 48.5 nm (PDI, 0.086), 70.6 nm (PDI, 0.179), and 74.9 nm (PDI, 0.225), respectively (Fig. 1A). To confirm the display of L_4-PHA molecule on BNCs, PHA–BNCs were immunoprecipitated with anti-HBsAg (S region) IgG-conjugated microbeads and subjected to Western blotting with HRP–SA. As shown in Fig. 1B, both bio-BNCs (about 45 and 48 kDa; the size difference is caused by glycosylation) and bio-PHA (about 30 kDa) were found to be coimmunoprecipitated, indicating that both molecules successfully form a complex on the surface of BNCs.

Identification of β1-6 GlcNAc in GnT-V-overexpressing cells

GnT-V-overexpressing stable cell lines WiDr and MKN45 (WiDr-GnT-V and MKN45-GnT-V) were analyzed by lectin blot and cytochemistry using L_4-PHA lectin. Increased amounts of β1-6 GlcNAc were found in 80- to 100-kDa and about 150- to 200-kDa proteins in the WiDr-GnT-V and MKN45-GnT-V cell lines, respectively (Fig. 2A, left). The protein profile of neither cell line was significantly changed by overexpression of GnT-V (Fig. 2A, right). GnT-V expression induced the change from β1-6 GlcNAc-free *N*-glycans to β1-6 GlcNAc-containing *N*-glycans, and it was considered that both amount and size of *N*-glycoproteins were not significantly affected by GnT-V expression. Cytochemical analyses using L_4-PHA lectin also confirmed that the expression of β1-6 GlcNAc on the cell surface is significantly enhanced in GnT-V-overexpressing cell lines (Fig. 2B). On the basis of the fluorescence intensity, the WiDr-GnT-V cell line was considered to express a greater amount of β1-6 GlcNAc on its surface compared with the MKN45-GnT-V cell line.

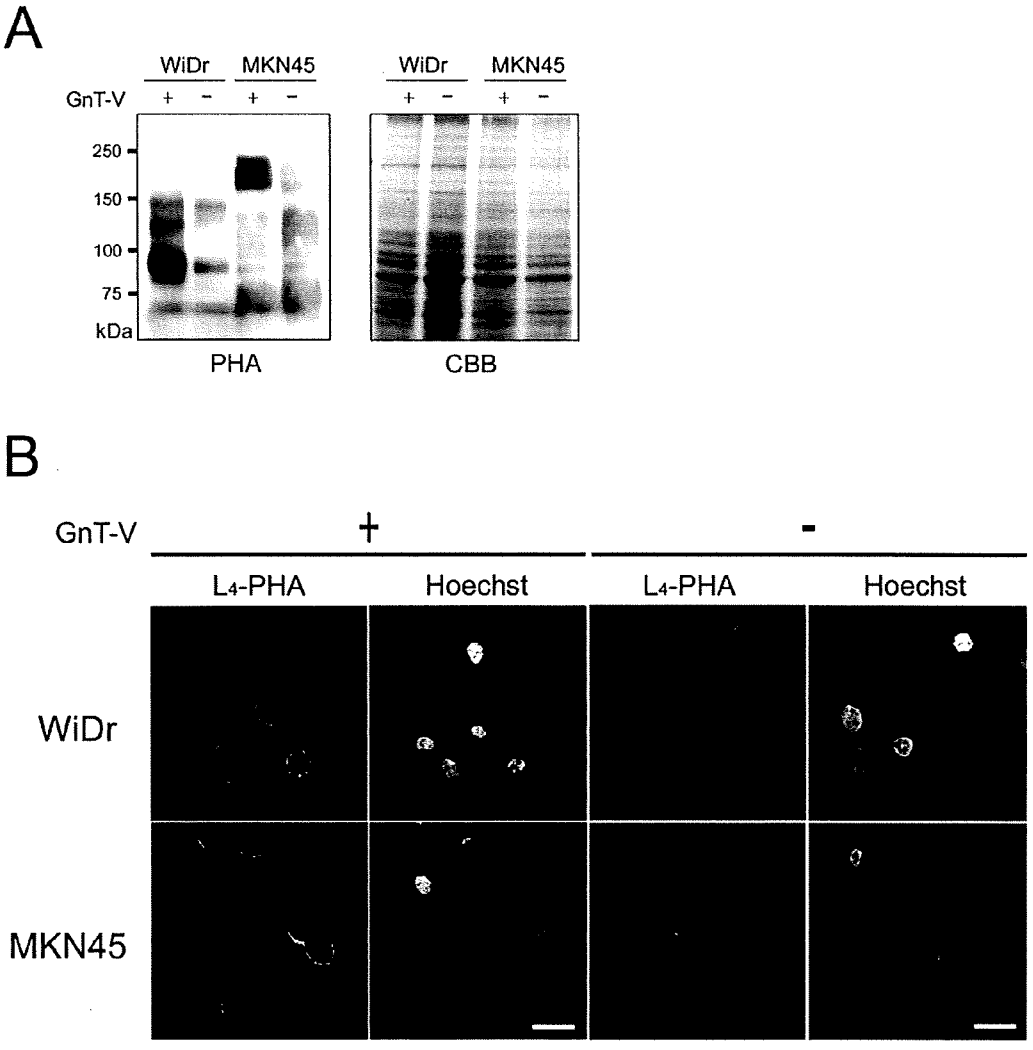

FIG. 2. Expression of β1-6 GlcNAc in GnT-V-overexpressing cells. (**A**) Ten micrograms (as protein) of total cell lysate (WiDr, MKN45 with/without GnT-V expression) was subjected to sodium dodecyl sulfate–polyacrylamide gel electrophoresis, and analyzed by lectin blotting with L_4-PHA (*left*) and Coomassie Brilliant Blue R-250 (CBB) staining (*right*). (**B**) Cytochemical analyses of GnT-V-overexpressing cells, using L_4-PHA lectin and Hoechst 33342. Scale bars: 20 μm.

L_4-PHA-mediated ex vivo *accumulation of BNCs*

To examine whether L_4-PHA could deliver BNCs to target cells *ex vivo*, the lipid bilayer moiety of PHA–BNCs was labeled with DiD, a membrane probe, and DiD-labeled PHA–BNCs were directly added to the culture medium of GnT-V-overexpressing cell lines. After 3 hr, strong DiD-derived fluorescence was found in both GnT-V-overexpressing cell lines (Fig. 3A). Cytotoxicity was not observed by phase-contrast imaging. This result suggested that a remarkable amount of PHA–BNCs accumulated in GnT-V-overexpressing cells, presumably through the interaction of L_4-PHA with cell surface β1-6 GlcNAc. The weak fluorescence observed in both parental cell lines might have been caused by endogenous β1-6 GlcNAc, as observed in Fig. 2A. Intriguingly, the fluorescence of the WiDr-GnT-V cell line was higher than that of the MKN45-GnT-V cell line, which may be due to the lower amount of β1-6 GlcNAc in the MKN45-GnT-V cell line (*see* Fig. 2B). Flow cytometric analysis (Fig. 3B) confirmed that the GnT-V-overexpressing cell lines showed stronger

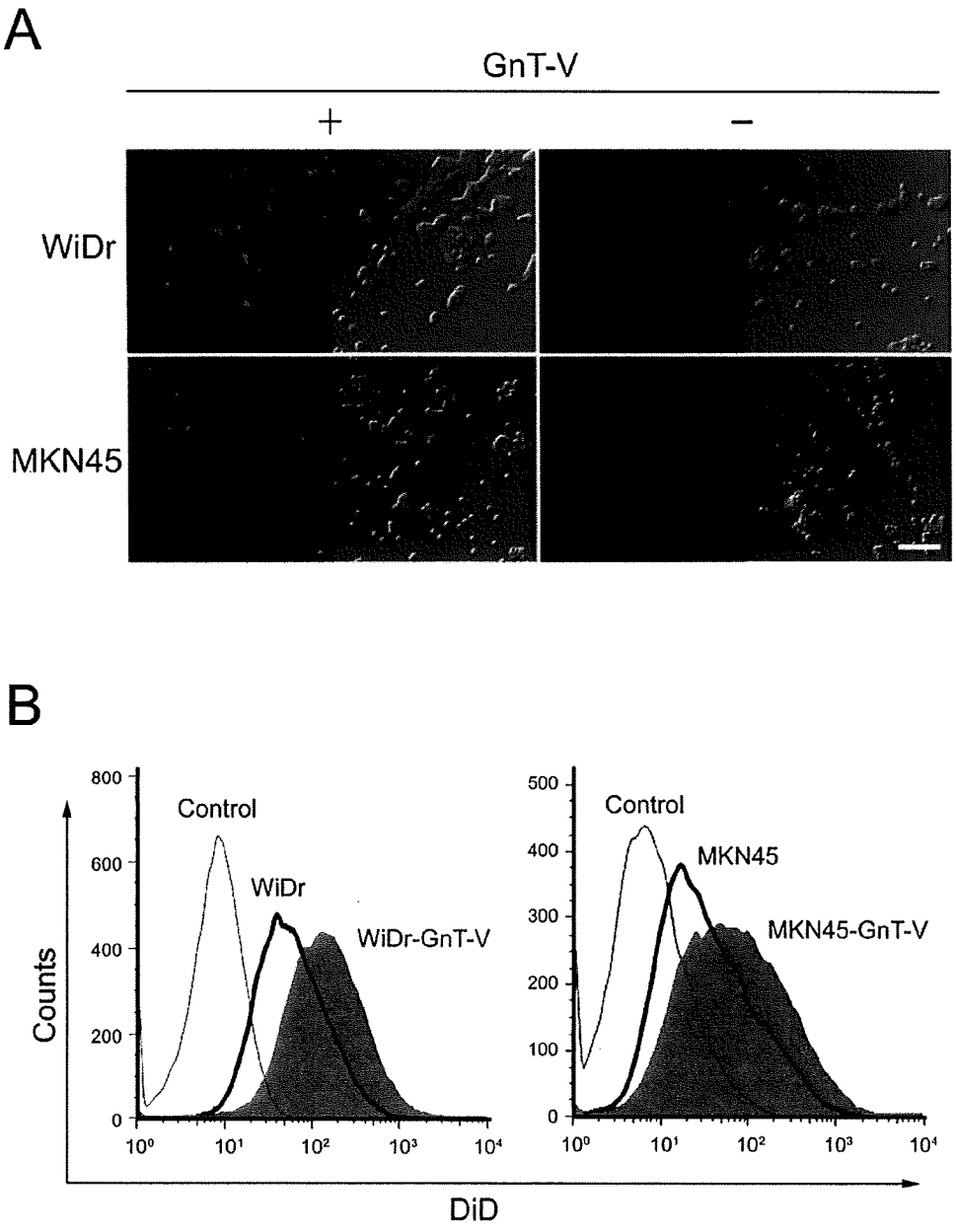

FIG. 3. L_4-PHA-mediated *ex vivo* accumulation of BNC. (**A**) Either GnT-V-overexpressing or parental cells of WiDr and MKN45 were incubated with DiD-labeled PHA–BNC, and then observed 3 hr after administration. Scale bar: 100 μm. (**B**) The cells incubated with DiD-labeled PHA–BNC were analyzed by flow cytometry. Untreated GnT-V-overexpresssing cells were used as control.

fluorescence intensity than parental WiDr and MKN45 cells. Geometric mean fluorescence intensity in GnT-V-overexpressing cells was approximately 2.6- and 1.9-fold higher than that of parental WiDr and MKN45 cells, respectively. Collectively, PHA–BNCs were shown to accumulate specifically with β1-6 GlcNAc-overexpressing cells *ex vivo* because of the targeting ability of L_4-PHA.

L_4-PHA-mediated in vivo *delivery of BNCs*

The mouse xenograft model harboring WiDr- and WiDr-GnT-V-derived tumors was used to evaluate the targeting ability of PHA–BNCs *in vivo*. Mice received systemic administration of DiD-labeled PHA–BNCs (40 μg as BNC protein) via the tail vein, and then the DiD-derived fluorescence from tumors was investigated with the *in vivo* optical imaging system 0, 1, 4, 8, 16, 24, and 48 hr after injection (Fig. 4A). Fluorescence was initially detected in WiDr-GnT-V-derived tumors at 1 hr, and reached a maximum at 24 hr (Fig. 4A, left). A slight increase in fluorescence was observed in WiDr-derived tumors during the observation period (Fig. 4A, right), implying that the enhanced permeability retention (EPR) effect is nearly undetectable in this system. To confirm the β1-6 GlcNAc-dependent accumulation of PHA–BNCs, mice were killed 24 hr after injection and tumors, hearts, and livers were isolated and observed with the *in vivo* optical imaging system. DiD-derived fluorescence was observed in both tumor types; GnT-V-overexpressing tumors showed higher fluorescence intensity than control tumors (Fig. 4B, top). However, the fluorescence intensities of both GnT-V-overexpressing and control liver showed no significant difference (Fig. 4B, bottom), indicating that PHA–BNCs might be equally trapped by the reticuloendothelial system (RES) in both livers. Among other major organs (spleen, kidney, heart, and lung), heart (Fig. 4B, middle) and kidneys showed weaker fluorescence than liver, but stronger than spleen and lungs. Regardless of the expression of GnT-V in tumors, there was no difference in the fluorescence of these organs. These results indicate that PHA–BNCs can efficiently accumulate in β1-6 GlcNAc-overexpressing tumor *in vivo* even by systemic administration.

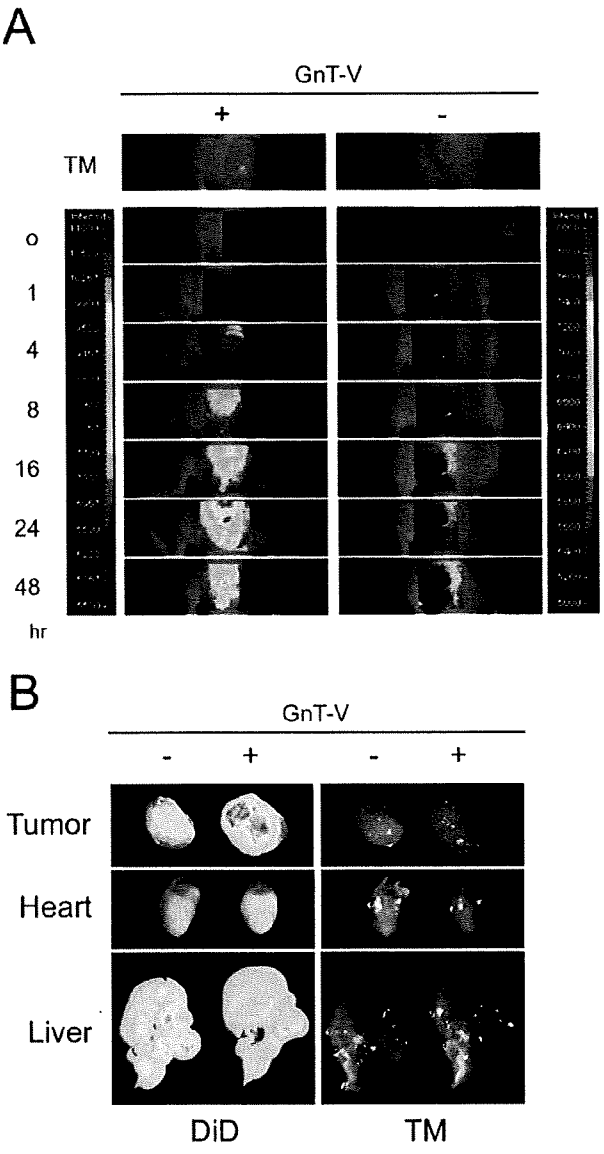

FIG. 4. L_4-PHA-mediated *in vivo* delivery of BNC. (A) The tumor region was observed with an *in vivo* imaging system after systemic administration of DiD-labeled PHA–BNC. The number of mice in each group was three. Similar results were obtained from each mouse. TM, transmission image. (B) Tumors, hearts, and livers were isolated and observed with an *in vivo* imaging system 24 hr after administration.

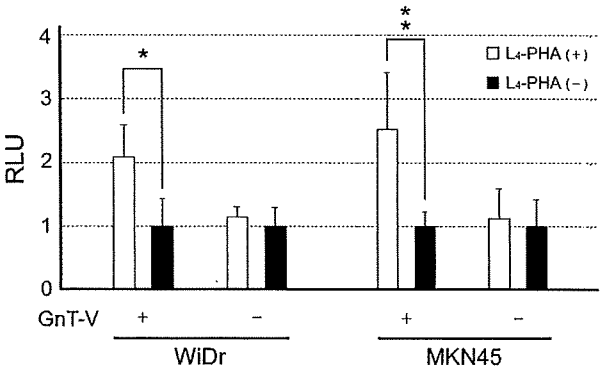

FIG. 5. L_4-PHA-mediated *ex vivo* gene delivery. Cells incubated with BNC–liposome complexes were lysed, and luciferase activity was measured. Results are presented as relative luminescence units (RLU) normalized to the protein concentration. The relative luminescence units derived for each cell line treated with bio-BNC–liposome complexes [L_4-PHA(–)] was set as 1 ($n = 4$; mean ± SD; t test, $^*p < 0.05$, $^{**}p < 0.005$).

L_4-PHA-mediated ex vivo *gene delivery*

Our studies have shown that BNCs form complexes with liposomes (Jung *et al.*, 2008), so that liposomes containing various materials (e.g., DNA, chemicals, or polystyrene beads) could be conjugated with BNCs, and then the BNC–liposome complexes could transport the incorporated payloads to target cells *ex vivo* and *in vivo*, based on the speci-

ficity of the BNCs. We therefore examined the transfection efficiency of a PHA–BNC–liposome complex to the malignant cancer cell lines WiDr-GnT-V and MKN45-GnT-V, using a luciferase gene as a reporter (Fig. 5). Both PHA–BNCs and bio-BNCs (negative control) showed similar luciferase activities in parental cell lines. PHA–BNCs were revealed to possess higher transfection efficiency to the GnT-V-overexpressing cell lines. Thus, PHA–BNC–liposome complexes can transport incorporated genes specifically to β1-6 GlcNAc-overexpressing malignant cell lines.

Discussion

Several lectins have so far been recognized as useful molecules for the diagnosis of various tumors *in situ* and *in vivo* (e.g., HPA [*Helix pomatia* agglutinin] for imaging tumors [Debbage *et al.*, 1998] and L_4-PHA in tumor diagnosis [Raedler and Schreiber, 1988] and in the treatment of cancers in human ([Wimer, 1997]). As for the delivery of anticancer drugs, a few attempts have been made with lectins. Wheat germ agglutinin (WGA)-conjugated liposomes have been used to deliver cisplatin to radiation-induced endothelial inflammatory areas in tumors by systemic administration (Geng *et al.*, 2004). However, the WGA-conjugated liposomes could not be used without the pretreatment with radiation. In this study, it was demonstrated that L_4-PHA is applicable for the targeting of BNCs to β1-6 GlcNAc-overexpressing malignant tumors *ex vivo* and *in vivo* without any additional pretreatment. Because expression of the β1-6 GlcNAc moiety is widely spread among highly metastatic tumors in humans (Fernandes *et al.*, 1991; Handerson and Pawelek, 2003; Dosaka-Akita *et al.*, 2004), PHA–BNCs are considered a promising nanodevice for either *in vivo* pinpoint gene/drug delivery in cancer therapy or bioimaging in cancer diagnosis.

The size of nanodevices in this field of research is generally important for *in vivo* systemic administration, because too large a device (>150 nm in diameter) will be removed from the bloodstream by the macrophages of the liver and spleen (i.e., RES) and too small a device (<40 nm in diameter) is also filtrated by the kidney (Drummond *et al.*, 1999). Moreover, the pore size of the tumor vasculature varies from 100 to 780 nm, which is larger than that of normal tissues (Hobbs *et al.*, 1998). Therefore, the diameter of nanodevices must be less than 200 nm for efficient capture by the tumor vasculature (i.e., EPR effect) (Sinn *et al.*, 2005). The average diameter of PHA–BNCs, about 75 nm (*see* Fig. 1A), is considered appropriate for *in vivo* tumor targeting. As shown in Fig. 4B, a substantial amount of PHA–BNCs was found to accumulate in the liver, indicating that RES unexpectedly entrapped PHA–BNCs. To avoid this entrapment and to improve the blood retention time, various nanodevices have been modified with polyethylene glycol (PEG) (Portney and Ozkan, 2006). The biodistribution of PHA–BNCs may be optimized by a PEG modification to achieve an effective cancer treatment.

BNC–liposome complexes could deliver incorporated payloads to specific cells and tissues *in vivo* by the targeting ability of BNCs (Jung *et al.*, 2008). In this study we generated bio-BNCs displaying L_4-PHA on their surface, which has allowed us to display various targeting molecules (e.g., cytokines, glycans, peptides, and antibodies) and to expand the applications of BNCs and BNC–liposome complexes. The transfection process based on BNCs and BNC–liposome complexes is postulated to consist of two steps. First, the target cell is recognized by the targeting molecules displayed on BNCs, such as the pre-S region for human hepatocytes (Yamada *et al.*, 2003; Iwasaki *et al.*, 2007; Jung *et al.*, 2008), EGF for EGFR-expressing cells (Yamada *et al.*, 2003), or anti-EGFR antibody for EGFR-expressing cells (Tsutsui *et al.*, 2007). Second, the disintegration of BNCs occurs on the cellular membrane followed by the action of membrane-fusion peptide sequences in pre-S and S regions (Berting *et al.*, 2000; Oess and Hildt, 2000), and the payloads are released into the cytoplasm (Jung *et al.*, 2008). Because PHA–BNC–liposome complexes successfully delivered DNA to GnT-V-overexpressing cells (*see* Fig. 5), presumably the complexes were captured by the β1-6 GlcNAc moiety on the target cells and then the payload was released to the cytoplasm.

As for tumor-directed *in vivo* delivery of nanodevices containing therapeutic materials to cancers, various targeting molecules have so far been displayed on the surface of such nanodevices, including antibodies (Schliemann and Neri, 2007), homing peptides (Zurita *et al.*, 2003), and aptamers (Ireson and Kelland, 2006). These molecules contribute to deliver the adjunct nanodevices by recognizing cell surface proteins; however, the recognition of targeting molecules is sometimes dependent on the species. This situation has hampered the development of these nanodevices for clinical use, although these nanodevices show high efficacy in animal models (Marshall, 2006). On the other hand, the structure of *N*-glycans is highly conserved between rodents and humans; in particular, the aberrant expression of β1-6 GlcNAc in malignant cancers has been observed in both murine models and humans. Our new strategy using lectins to target abnormal glycans, as hallmarks of malignant cancer, may indicate a novel DDS for cancer therapy.

Acknowledgments

The authors thank Dr. T. Yamada (Beacle, Inc.), Prof. M. Seno (Okayama University), Prof. A. Kondo (Kobe University), and Prof. M. Ueda (Keio University, Medical School) for helpful advice. The authors are also grateful to Ms. Y. Matsushita for technical support. This work was supported in part by Grants-in-Aid for Scientific Research on Priority Areas (18015032) from the Ministry of Education, Culture, Sports, Science, and Technology of Japan; Creation of Bio-Devices and Bio-Systems with Chemical and Biological Molecules for Medical Use (CREST) and the Regional Research and Development Resources Utilization Program of the Japan Science and Technology Agency (JST); and by Grants-in-Aid for Research on Advanced Medical Technology from the Ministry of Health, Labor, and Welfare.

Author Disclosure Statement

No competing financial interests exist.

References

Abdullaev, F.I., and De Mejia, E.G. (1997). Antitumor effect of plant lectins. Natural Toxins 5, 157–163.

Berting, A., Fischer, C., Schaefer, S., Garten, W., Klenk, H.D., and Gerlich, W.H. (2000). Hemifusion activity of a chimeric in-

fluenza virus hemagglutinin with a putative fusion peptide from hepatitis B virus. Virus Res. 68, 35–49.

Buckhaults. P., Chen, L., Freigen, N., and Pierce, M. (1997) Transcriptional regulation of *N*-acetylglucosaminyltransferase V by the *src* oncogene. J. Biol. Chem. 272, 19575–19581.

Chen, L., Zhang, W., Fregien, N., and Pierce, M. (1998). The Her-2/*neu* oncogene stimulates the transcription of *N*-acetylglucosaminyltransferase V and expression of its cell surface oligosaccharide products. Oncogene 17, 2087–2093.

Cummings, R.D., and Kornfeld, S. (1982). Characterization of the structural determinants required for the high affinity interaction of asparagine-linked oligosaccharides with immobilized *Phaseolus vulgaris* leukoagglutinating and erythroagglutinating lectins. J. Biol. Chem. 257, 11230–11234.

Debbage, P.L., Griebel, J., Ried, M., Gneiting, T., De Vries, A., and Hulzler, P. (1998). Lectin intravital perfusion studies in tumor-bearing mice: Micrometer-resolution, wide-area mapping of microvascular labeling, distinguishing efficiently and inefficiently perfused microregions in the tumor. J. Histochem. Cytochem. 46, 627–639.

De Meyer, S., Depla, E., Maertens, G., Soumillion, S., and Yap, S.H. (1999). Characterization of small hepatitis B surface antigen epitopes involved in binding to human annexin V. J. Viral Hepat. 6, 277–285.

Dennis, J.S., Pawling, J., Cheung, P., Partridge, E., and Demetriou, M. (2002). UDP-*N*-acetylglucosamine:α-6-D-mannoside β1,6 *N*-acetylglucosaminyltransferase V (Mgat5) deficient mice. Biochim. Biophys. Acta 1573, 414–422.

Dennis, J.W., Granovsky, M., and Warren, C.E. (1999). Glycoprotein glycosylation and cancer progression. Biochim. Biophys. Acta 1473, 21–34.

Dosaka-Akita, H., Miyoshi, E., Suzuki O., Itoh, T., Katoh, H., and Taniguchi, N. (2004). Expression of *N*-acetylglucosaminyltransferase V is associated with prognosis and histology in non-small cell lung cancers. Clin. Cancer Res. 10, 1773–1779.

Drummond, D.C., Meyer, O., Hong, K., Kirpotin, D., and Papahadjopoulos, D. (1999). Optimizing liposomes for delivery of chemotherapeutic agents to solid tumors. Pharm. Rev. 51, 691–743.

Fernandes, B., Sagman, U., Auger, M., Demetriou, M., and Dennis, J.W. (1991). β1-6 branched oligosaccharides as a marker of tumor progression in human breast and colon neoplasia. Cancer Res. 51, 718–723.

Geng, L., Osusuky, K., Konjeti, S., Fu, A., and Hallahan, D. (2004). Radiation-guided drug delivery to tumor blood vessels results in improved tumor growth delay. J. Control. Release 99, 369–381.

Granovsky, M., Faya, J., Pawling, J., Mullar, J., Khokha, R., and Dennis, J.W. (2000). Suppression of tumor growth and metastasis in Mgat5-deficient mice. Nat. Med. 6, 306–312.

Hakomori, S. (1989). Aberrant glycosylation in tumors and tumor-associated carbohydrate antigens. Adv. Cancer Res. 52, 257–331.

Handerson, T., and Pawelek, J.M. (2003). β1,6-branched oligosaccharides and coarse vesicles: A common, pervasive phenotype in melanoma and other human cancers. Cancer Res. 63, 5363–5369.

Hobbs, S.K., Monsky, W.L., Yuan, F., Roberts, W.G., Griffith, L., Torchilin, V.P., and Jain, R.K. (1998). Regulation of transport pathways in tumor vessels: Role of tumor type and microenvironment. Proc. Natl. Acad. Sci. U.S.A. 95, 4607–4612.

Ihara, S., Miyoshi, E., Ko, J.H., Murata, K., Nakahara, S., Honke, K., Dickson, R.B., Lin, C.Y., and Taniguchi, N. (2002). Prometastatic effect of *N*-acetylglucosaminyltransferase V is due to modification and stabilization of active matriptase by adding β1-6 GlcNAc branching. J. Biol. Chem. 277, 16960–16967.

Ireson, C.R., and Kelland, L.R. (2006). Discovery and development of anticancer aptamers. Mol. Cancer Ther. 12, 2957–2962.

Iwasaki, Y., Ueda, M., Yamada, T., Kondo, A., Seno, M., Tanizawa, K., Kuroda, S., Sakamoto, M., and Kitajima, M. (2007). Gene therapy of liver tumors with human liver-specific nanoparticles. Cancer Gene Ther. 14, 74–81.

Jung, J., Matsuzaki, T., Tatematsu, K., Okajima, T., Tanizawa, K., and Kuroda, S. (2008). Bio-nanocapsule conjugated with liposomes for *in vivo* pinpoint delivery of various materials. J. Control. Release 126, 255–264.

Ko, J.H., Miyoshi, E., Noda, K., Ekuni, A., Kang, R., Ikeda, Y., and Taniguchi, N. (1999). Regulation of the GnT-V promoter by transcription factor Ets-1 in various cancer cell lines. J. Biol. Chem. 274, 22941–22948.

Kuroda, S., Otaka, S., Miyazaki, T., Nakao, M., and Fujisawa, Y. (1992). Hepatitis B virus envelope L protein particles: Synthesis and assembly in *Saccharomyces cerevisiae*, purification and characterization. J. Biol. Chem. 267, 1953–1961.

Marshall, E. (2006) Violent reaction to monoclonal antibody therapy remains a mystery. Science 311, 1688–1689.

Mehdi, H., Kaplan, M.J., Anlar, F.Y., Yang, X., Bayer, R., Sutherland, K., and Peeples, M.E. (1994). Hepatitis B virus surface antigen binds to apolipoprotein H. J. Virol. 68, 2415–2424.

Murata, K., Miyoshi, E., Kameyama, M., O. Ishikawa, Kabuto, T., Sasaki, Y., Hiratsuka, M., Ohigashi, H., Ishiguro, S., Ito, S., Honda, H., Takemura, F., Taniguchi, N., and Imaoka, S. (2000). Expression of *N*-acetylglucosaminyltransferase V in colorectal cancer correlates with metastasis and poor prognosis. Clin. Cancer Res. 6, 1772–1777.

Murata, K., Miyoshi. E., Ihara, Noura, S., Kameyama, M., Ishikawa, O., Doki, Y., Yamada, T., Ohigashi, H., Sasaki, Y., Higashiyama, M., Tarui, T., Takeda, Y., Kannagi, R., Taniguchi, N., and Imaoka, S. (2004). Attachment of human colon cancer cells to vascular endothelium is enhanced by *N*-acetylglucosaminyltransferase V. Oncology 66, 492–501.

Neurath, A.R., Kent, S.B., Strick, N., and Parker, K. (1986). Identification and chemical synthesis of a host cell receptor binding site on hepatitis B virus. Cell 46, 429–436.

Oess, S., and Hildt, E. (2000). Novel cell permeable motif derived from the PreS2-domain of hepatitis-B virus surface antigens. Gene Ther. 7, 750–758.

Portney, N.G., and Ozkan, M. (2006). Nano-drug delivery, imaging, and sensing. Anal. Bioanal. Chem. 384, 620–630.

Raedler, A., and Schreiber, S. (1988). Analysis of differentiation and transformation of cells by lectins. Crit. Rev. Clin. Lab. Sci. 26, 153–193.

Schliemann, C., and Neri, D. (2007). Antibody-based targeting of the tumor vasculature. Biochim. Biophys. Acta 1776, 175–192.

Sinn, P.L., Sauter, S.L., and McCray, P.B., Jr. (2005). Gene therapy progress and prospects: Development of improved lentiviral and retroviral vectors: design, biosafety, and production. Gene Ther. 12, 1089–1098.

Tsutsui, Y., Tomizawa, K., Nagita, M., Michiue, H., Nishiki, T., Ohmori, I., Seno, M., and Matsui, M. (2007). Development of bionanocapsules targeting brain tumors. J. Control. Release 122, 159–164.

Wimer, B.M. (1990). Therapeutic activities of PHA-L_4, the mitogenic isolectin of phytohemagglutinin. Mol. Biother. 2, 74–90.